การย่อยสลายไดยูรอนด้วยกระบวนการออกซิเดชันขั้นสูงเชิงไฟฟ้าเคมี

นางสาวปัญชิกา ประภากรรัตนา

วิทยานิพนธ์นี้เป็นส่วนหนึ่งของการศึกษาตามหลักสูตรปริญญาวิศวกรรมศาสตรมหาบัณฑิต
สาขาวิชาวิศวกรรมเคมี ภาควิชาวิศวกรรมเคมี
คณะวิศวกรรมศาสตร์ จุฬาลงกรณ์มหาวิทยาลัย
ปีการศึกษา 2559
ลิขสิทธิ์ของจุฬาลงกรณ์มหาวิทยาลัย

DEGRADATION OF DIURON VIA ELECTROCHEMICAL ADVANCED OXIDATION
PROCESS

Miss Panchika Prapakornrattana

A Thesis Submitted in Partial Fulfillment of the Requirements

for the Degree of Master of Engineering Program in Chemical Engineering

Department of Chemical Engineering

Faculty of Engineering

Chulalongkorn University

Academic Year 2016

Thesis Title DEGRADATION OF DIURON VIA ELECTROCHEMICAL ADVANCED OXIDATION PROCESS

By Miss Panchika Prapakornrattana

Field of Study Chemical Engineering

Thesis Advisor Associate Professor Varong Pavarajarn, Ph.D.

Accepted by the Faculty of Engineering, Chulalongkorn University in Partial Fulfillment of the Requirements for the Master's Degree

....Dean of the Faculty of Engineering

(Associate Professor Supot Teachavorasinskun, D.Eng.)

THESIS COMMITTEE

....Chairman

(Assistant Professor Apinan Soottitantawat, D.Eng.)

....Thesis Advisor

(Associate Professor Varong Pavarajarn, Ph.D.)

....Examiner

(Associate Professor Sarawut Rimdusit, Ph.D.)

....External Examiner

(Chanchana Thanachayanont, Ph.D.)

ปัญชิกา ประภากรรัตนา : การย่อยสลายไดยูรอนด้วยกระบวนการออกซิเดชันขั้นสูงเชิง
ไฟฟ้าเคมี (DEGRADATION OF DIURON VIA ELECTROCHEMICAL ADVANCED
OXIDATION PROCESS) อ.ที่ปรึกษาวิทยานิพนธ์หลัก: รศ. ดร. วรงค์ ปวราจารย์, 87
หน้า.

ไดยูรอนเป็นหนึ่งในยาปราบวัชพืชที่ใช้กันทั่วไปในประเทศไทย เนื่องจากความเป็นพิษสูง
และใช้เวลาในการสลายตัวตามธรรมชาตินาน ทำให้เกิดเป็นปัญหาการปนเปื้อนในสิ่งแวดล้อม
การวิจัยนี้มุ่งเน้นถึงการย่อยสลายไดยูรอนด้วยกระบวนการออกซิเดชันขั้นสูงเชิงไฟฟ้าเคมีซึ่ง
อนุมูลไฮดรอกซิล ถูกผลิตขึ้นเมื่อจ่ายกระแสไฟฟ้าผ่านขั้วไฟฟ้าที่แช่อยู่ในสารละลาย อิทธิพลของ
ความเร็วในการปั่นกวน ชนิดของสารอิเล็คโตรไลต์ กระแสไฟฟ้าที่ป้อนเข้าในระบบ ค่าความเป็น
กรด-ด่างเริ่มต้น ประเภทของขั้วไฟฟ้า และอุณหภูมิได้ถูกตรวจสอบ ผลการศึกษาพบว่าถึง ไดยู
รอนสามารถสลายตัวไปได้ถึง 95% ภายใน 6 ชั่วโมงของการเกิดปฏิกิริยา ปฏิกิริยาในการย่อย
สลายเป็นไปตามจลนศาสตร์อันดับที่หนึ่ง โดยการย่อยสลายไดยูรอนจะเพิ่มขึ้นเมื่อกระแสไฟฟ้าที่
ป้อนเข้าระบบเพิ่มขึ้น อุณหภูมิมีค่าเพิ่มขึ้น หรือค่าความเป็นกรด-ด่างเริ่มต้นลดลง นอกจากนี่
อิทธิพลของแอนไอออนยังส่งผลกระทบต่อการย่อยสลายไดยูรอนอีกด้วย

ภาควิชา	วิศวกรรมเคมี	ลายมือชื่อนิสิต	
สาขาวิชา	วิศวกรรมเคมี	ลายมือชื่อ อ.ที่ปรึกษาหลัก	
ปีการศึกษา	2559		

5770221921 : MAJOR CHEMICAL ENGINEERING

KEYWORDS: DIURON DEGRADATION/ ELECTROCHEMICAL ADVANCED OXIDATION PROCESS

PANCHIKA PRAPAKORNRATTANA: DEGRADATION OF DIURON VIA ELECTROCHEMICAL ADVANCED OXIDATION PROCESS. ADVISOR: ASSOC. PROF. VARONG PAVARAJARN, Ph.D., 87 pp.

Diuron is one of common herbicides used in Thailand. Due to its persistence and its potent toxicity, diuron contamination becomes a very serious environmental problem. This research focuses on degradation of diuron via electrochemical advanced oxidation process (EAOP), in which reactive hydroxyl radicals are produced when electrical current is supplied to electrodes immersed in the solution. The influence of mixing speed, type of electrolyte, applied electric current, initial pH, type of electrode, and temperature were investigated. The results showed that up to 95% of diuron could be degraded within 6 hours of the reaction. The reaction generally follows the pseudo-first-order kinetic. The diuron degradation increased with increasing applied electric current, also increasing temperature, or decreasing pH of the solution. Moreover, type of anion affects the diuron degradation.

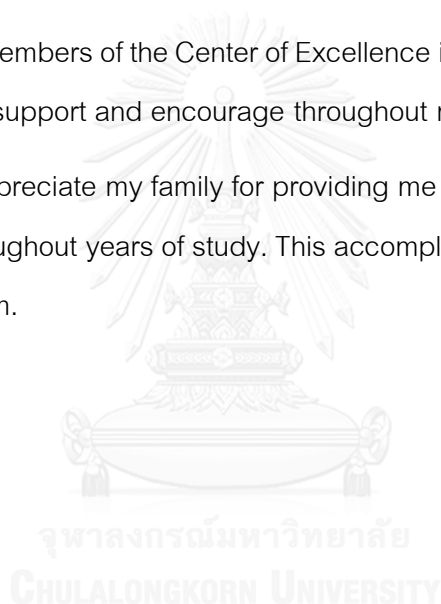|		
Department:	Chemical Engineering	Student's Signature
Field of Study:	Chemical Engineering	Advisor's Signature
Academic Year:	2016	

ACKNOWLEDGEMENTS

จุฬาลงกรณ์มหาวิทยาลัย
CHULALONGKORN UNIVERSITY

CONTENTS

LIST OF TABLES

LIST OF FIGURES

CHAPTER I

INTRODUCTION

Thailand is an agricultural country which has been farming for a long time. The agricultural activities have several types such as planting, farming, and cultivation. Currently, the agricultures have used herbicides to eliminate weed.

Diuron [3-(3,4-dichlorophenyl)-1,1-dimethylurea] is a common herbicide that is used for weed elimination. It inhibits photosynthesis process by preventing formation of oxygen and obstructing the electron transfer at the level of photosystem II of photosynthetic micro-organisms and plants. Diuron requires significant long decomposition time due to long half-life. Diuron is a pollutant that can be found in the environment such as soil, sediment, and water. It has a high toxicity. This work focus on contaminate into water because it is a medium that can be spread to others.

The removal of diuron can beconducted via many techniques such as hydrolysis, biodegradation, photodegradation, adsorption, and advanced oxidation processes (AOPs). The AOPs is one of highly efficient techniques for wastewater treatment. The AOPs depend on formation of hydroxyl radicals ($^{\bullet}$OH). The hydroxyl radical is a powerful oxidant which can destroy organic pollutants until complete mineralization into carbon dioxide, water, and intermediates.

Nowadays, this traditional technique has been developed and become a new application so-called electrochemical advanced oxidation processes (EAOPs) [1, 2]. The EAOPs have several advantages such as high efficiency, easy handling, safety, and

versatility. These methods can remove pollutants with COD in a range of 0.01 to 100 g·L^{-1} , as shown in Figure 1.1 [2]..
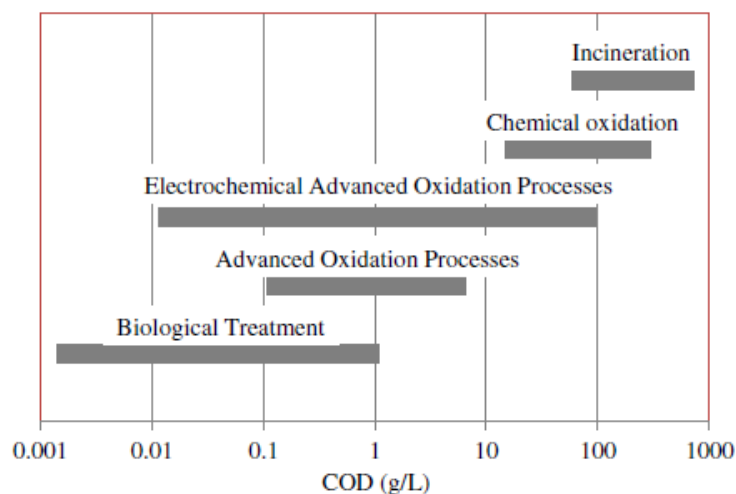
Figure 1.1 Wastewater treatment based on the amount of organic pollutant [2].

This research focuses on the degradation of diuron via the electrochemical advanced oxidation processes (EAOPs). The aim is to study the behavior of diuron degradation via the electrochemical advanced oxidation processes (EAOPs).

This thesis can be divided into 5 chapters as followed:

Chapter I proposes the motivation and introduction of this research.

Chapter II explains the theory and literature reviews related to physical properties of diuron, electrochemical advanced oxidation processes.

Chapter III describes the chemicals, equipment, apparatus experimental procedures and analytical method.

Chapter IV describes experiment results and discussion.

Chapter V summarizes the results and recommends.

CHAPTER II

THEORY AND LITERATURE REVIEWS

This chapter describes the theory and literature reviews related to chemical and physical properties of diuron, electrochemical oxidation processes and electrochemical advanced oxidation processes.

2.1 Diuron

Diuron (3-(3,4-dichlorophenyl)-1,1-dimethylurea) or DCMU is a herbicide in phenylamide family and a subclass of phenylurea. The empirical formula is $C_9H_{10}Cl_2N_2O$. The structure formula is shown in Figure 2.1. Diuron is a white crystalline and odorless solid. It is stable at room temperature, and is hydrolyzed by acid and alkalis. The physical and chemical properties described in Table 2.1.
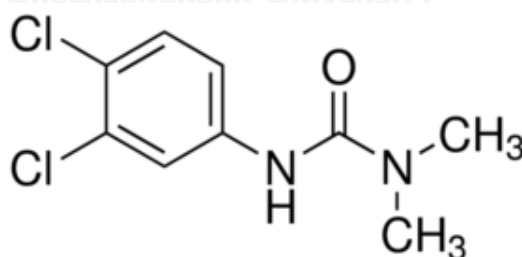
Figure 2.1 Chemical structure of diuron.

Table 2.1 Physical and chemical properties of diuron.

Characteristics	Detailes
Common name	Diuron or DCMU
Chemical name – IUPAC	3-(3,4-dichlorophenyl)-1,1-dimethylurea
Chemical name – CAS	N'-(3,4-dichlorophenyl)-N,N-dimethylurea
CAS number	330-54-1
Empirical formula	$C_9H_{10}Cl_2N_2O$
Molecular weight	233.09 g/mol
Bulk density	1.48 g/cm^3
Boiling point	180 – 190 ºC
Melting point	158 – 159 ºC
Vapor pressure (at 25 ºC)	0.009 mPa
Solubility in water (at 25 ºC)	36.4 mg/l
Henry's constant (at 25 ºC)	7.0 × 10-6 Pa m^3/mol
Fugacity ratio	0.04

Diuron is a product of hill reaction by reacting between 3,4-dichlorophenyl isocyanate and dimethylamine. It was utilized the first time in 1951 and was merchandised by E.I. du Pont de Nemours and Co (now DuPont) in 1954. Diuron is often used in combination with other herbicides such as bromacil, hexazinone, paraquat, and etc. Today, diuron is a famous herbicide that is utilized for weed elimination. The principle is to inhibit photosynthesis process by blocking oxygen production [3] and obstructing the electron transfer at the level of photosystem II (P700) of photosynthetic micro-organisms and plants.

Diuron has a long half-life, i.e. 200 days in soil and 90 days in water [4]. It can be found in environment such as soil, water, and sediment [5, 6]. So, diuron is source of pollutant in soil and aquatic environmental. Moreover, diuron is slightly toxic to mammals. It can be absorbed into the gastrointestinal and respiratory systems. Moreover, it can be accumulated in fat, muscle, liver, and kidney.

2.2 Electrochemical advanced oxidation processes

In recent years, the new advance oxidation process (AOP) is developed which based on the electrochemical technology that is called electrochemical advanced oxidation processes (EAOPs) [1]. The EAOPs is used for removal of organic pollutants from wastewater.

The electrochemical advanced oxidation process has several advantages such as high efficiency, easy handling, safety, and versatility. The main disadvantages of these technology are the cost of electrical supply, the low conductance, the loss of activity, and shortening of the electrode lifetime by fouling due to the deposition of organic material on surface.

The electrochemical oxidation methods can be subdivided in 2 mainly types as follow [7]:

1) Direct anodic oxidation

2) Indirect anodic oxidation

The electrochemical advanced oxidation processes can occur directly at anodes through the generation of physically adsorbed active oxygen. This process is called anodic oxidation or direct anodic oxidation. The mechanism of this process is based on intermediates of oxygen formation in aqueous media [5, 8-11]. The process involves anodic oxygen transfer from water to organics via hydroxyl radical formed by water electrolysis [12].

Hydroxyl radicals ($^{\bullet}OH$) are formed via the oxidation on anode surface, as shown in equation 2.1. The $^{\bullet}OH$ is rarely found in the reaction media because it reacts with another components before forming oxygen. In addition, it may be transformed into hydrogen peroxide and hydroperoxyl radical, as shown in equation 2.2 and 2.3 [13].

$$H_2O \longrightarrow {^{\bullet}OH} + H^+ + e^- \qquad\qquad 2.1$$

$$^{\bullet}OH + {^{\bullet}OH} \longrightarrow H_2O_2 \qquad\qquad 2.2$$

$$H_2O_2 + {^{\bullet}OH} \longrightarrow HO_2^{\bullet} + H_2O \qquad\qquad 2.3$$

The hydroxyl radical ($^{\bullet}OH$) is a highly effective oxidant (Table 2.2) which is able to non-selectively destroy organic and organometallic contaminants until complete mineralization into carbon dioxide (CO_2), water (H_2O), and inorganic ions. The $^{\bullet}OH$ can destroy diuron via hydroxylation, dehydrogenation, demethylation or dehalogenation [2, 14], as shown in equation 2.4.

$$Diuron + {^{\bullet}OH} \longrightarrow Diuron\ minerization\ products \qquad\qquad 2.4$$

Table 2.2 Standard potential of some oxidizing species [2].

Oxidizing agent	Standard potential (V vs. SHE)
Oxygen (molecular)	1.23
Oxygen (atomic)	2.42
Chlorine dioxide	1.27
Chlorine	1.36
Hydroxyl radical	2.80
Ozone	2.08
Florine	3.06
Positively charged hole on TiO_2	3.20

The diuron degradation occurs on the anode surface. This process can be divided into 3 main stages: 1) pollutant transfer from bulk solution to anode surface, 2) electrodic reaction or mediated oxidation by hydroxyl radicals, and 3) oxidized product transfer from anode surface to bulk solution. The schematic diagram of mechanism of diuron degradation via electrochemical advanced oxidation process (EAOP) is shown in Figure 2.2 [15].
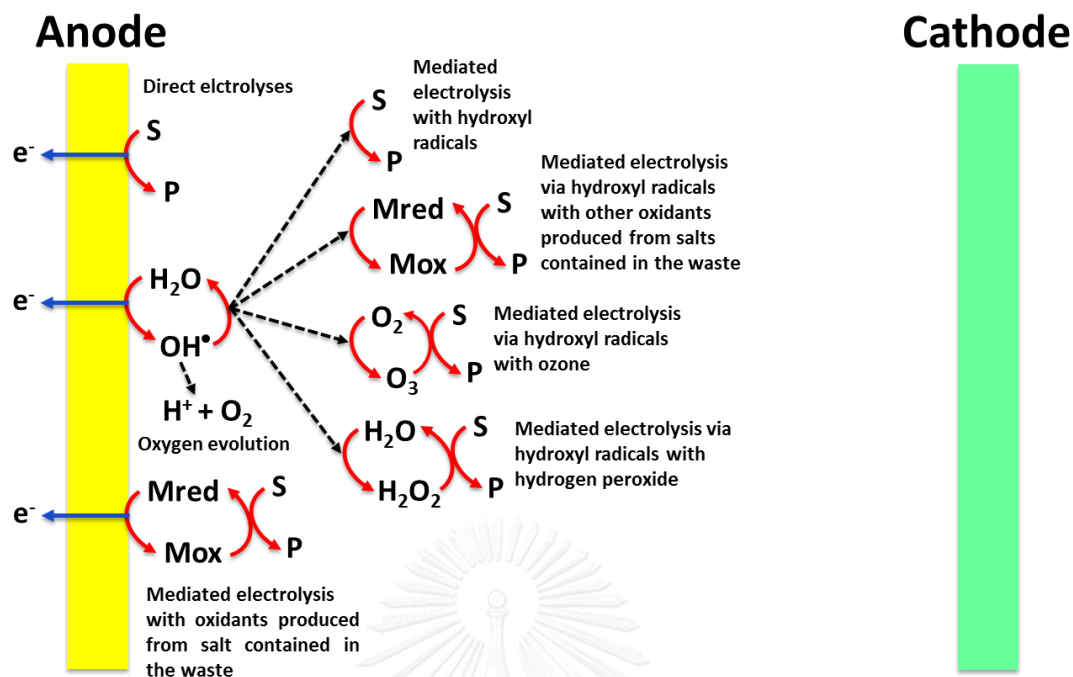
Figure 2.2 Schematic diagram of mechanism of diuron degradation via EAOP [15].

The efficiency of diuron degradation depends on several variables as followed:

2.2.1 Electrode

The electrode for electrochemical advanced oxidation process is a non-active electrode, which is the electrode material that does not change the oxidation number during the reaction. The most non-active electrodes are doped SnO_2, PbO_2, boron doped diamond (BDD), and doped and sub-stoichiometric TiO_2. The process is shown in equation 2.5 [12, 16]:

$$M[\ ] + H_2O \longrightarrow M[^\bullet OH] + H^+ + e^- \qquad\qquad 2.5$$

where $M[\ ]$ is an electrode surface site.

$M[^\bullet OH]$ is a hydroxyl radical that occurs physisorption at a surface site.

The oxygen on non-active electrode is occurred through the reaction between an additional H_2O and $M[^\bullet OH]$ site, as shown in equation 2.6 [12, 16]:

$$M[^\bullet OH] + H_2O \longrightarrow M[\ ] + O_2 + 3H^+ + e^-$$ 2.6
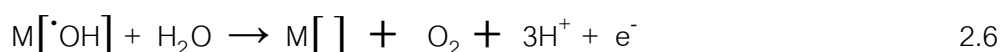
The non-active electrode can produce high concentrate hydroxyl radicals, but not all electrodes cleanly without toxic substance. The advantages and disadvantage of each electrode is different. The example electrodes that be used for EAOPs is shown in Table 2.3.

For the active anode, there is a strong interaction between hydroxyl radical ($^\bullet OH$) and electrode (M). The transition of the oxygen (O_2) from hydroxyl radical ($^\bullet OH$) to surface electrode (M) results a higher metal oxide (MO) as shown in equation 2.7. The surface redox couple MO/M acts as a mediator in the selective oxidation of organic compound on the active anode as shown in equation 2.8 [12, 16]:

$$M[^\bullet OH] \longrightarrow MO + H^+ + e^-$$ 2.7

$$MO + R \longrightarrow M + RO$$ 2.8

The side reaction of oxygen evolution is the chemical decomposition of higher metal oxide, as shown in equation 2.9 [12, 16]:

$$MO \longrightarrow M + \frac{1}{2}O_2$$ 2.9

Table 2.3 The advantages and disadvantage of each electrode.

Type of electrodes	Advantages	Disadvantages
Doped-SnO_2 electrodes	- non-active	- low conductivity - short lifetime
PbO_2 electrodes	- non-activeand stable - high efficiency - good corrosion resistance - long lifetime - low cost	- The mechanism of formation ˙OH has still to be understood.
Doped and sub-stoichiometric TiO_2 electrodes	- non-activeand stable - very high electrical conductivity	- brittle
Boron-doped diamond electrodes	- non-activeand stable - high current density - high conductivity - long lifetime	- high cost
Graphite	- inactive	- low current density

2.2.2 Applied Current

The applied current is one of the important variables that can affect the oxidation process [13, 16, 17]. The formation of hydroxyl radical ($^{\bullet}$OH) depends on applied current. Increasing applied current increases the efficiency of electrochemical process. The process is favored at low current density [18, 19].

2.2.3 Initial pH of solution

The initial pH is one of main parameters that affects EAOP. The pH affects the formation of active species and reaction with pollutants [20]. The generation of hydroxyl radical via water oxidation is favored at pH lower than 9 [21]. In the basic solution, the hydroxyl radicals behave like a weak acid and interact with the hydroxide (OH$^-$) to form O$^-$, as followed in equation 2.10 [22]:

$$^{\bullet}OH + OH^- \leftrightarrow O^- + H_2O^{\bullet} \qquad\qquad 2.10$$

2.2.4 Temperature

Increasing temperature can reduce time of operation whereas the degradation of diuron is almost complete mineralization [23]. The efficiency of diuron degradation increases with temperature.

2.2.5 Electrolyte

The type of electrolytes was an important parameter. Electrolytes helped for increasing conductivity and decreasing resistance [24]. The electrolytes affect kinetic and degradation pathway. The common of electrolytes used in EAOP are sodium chloride (NaCl), sodium sulfate (Na_2SO_4), sodium nitrate ($NaNO_3$), and sodium carbonate (Na_2CO_3). Some electrolytes can produce the oxidants which participate in the reaction.

2.3 Diuron degradation pathway

The degradation of diuron has many techniques, as followed:

2.3.1 Hydrolysis

Diuron has a slow rate of hydrolysis at the 25 °C. Diuron is catalyzed by acid-base and formed the zwitterion. After that, the zwitterion becomes 3,4-dichlorophynyl isocyanate and dimethylamine. The hydrolysis reaction is an irreversible reaction. The product is occurred 3,4-dichloroaniline and carbon dioxide [25, 26].
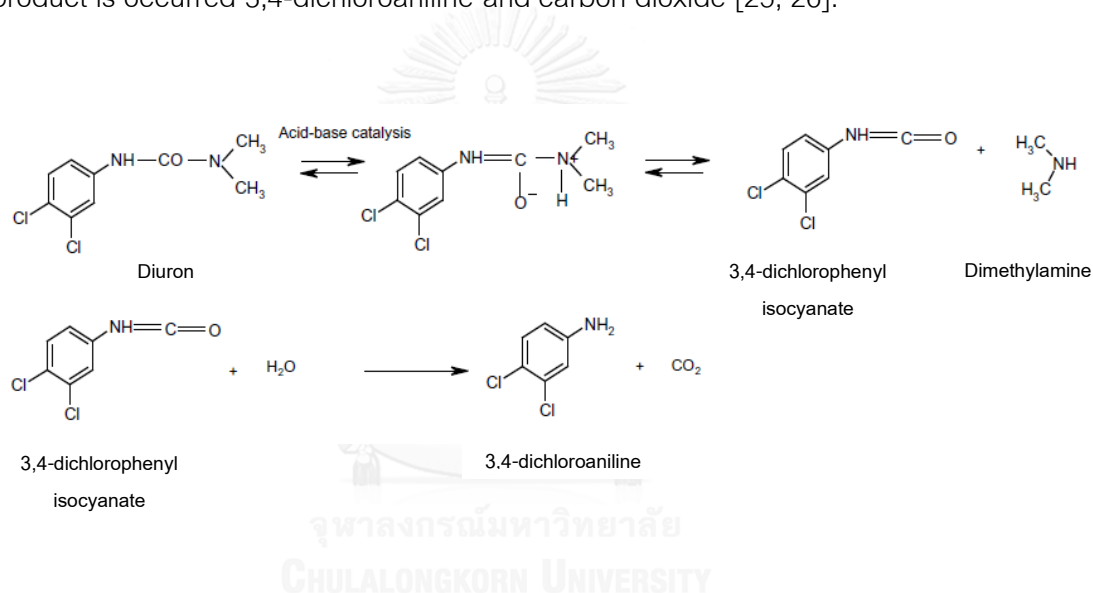
Figure 2.3 Scheme of hydrolysis pathway of diuron [25, 26].

2.3.2 Biodegradations

This method uses bacteria or fungi for degradation of organic compound. Figure 2.4 is shown degradation pathway by bacteria. The bacteria which utilized are shown in Table 2.4. This study can be divided 2 mainly parts as follow, degradation of diuron and 3,4-dichloroaniline [25, 27].
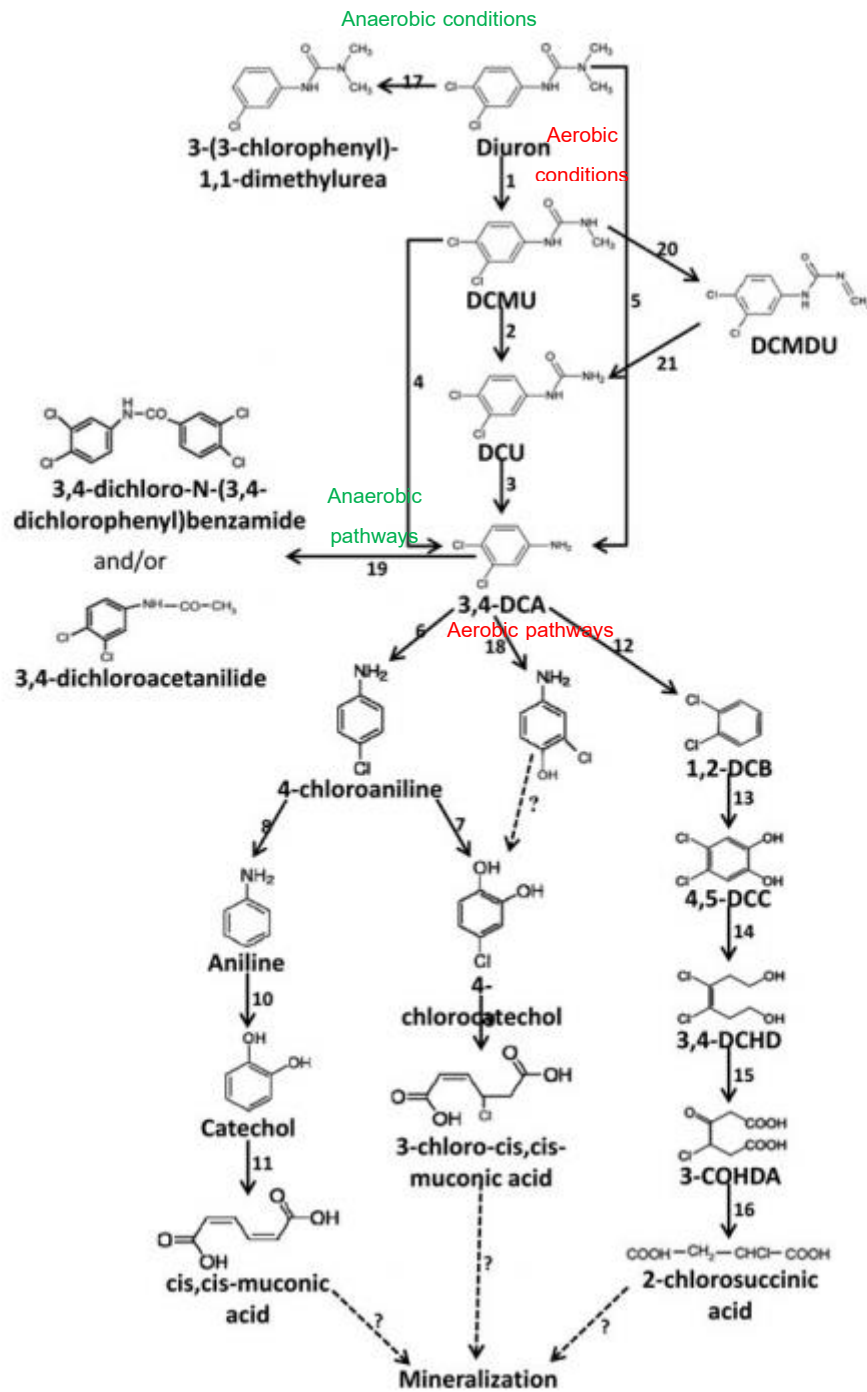
Figure 2.4 Metabolic pathways of biodegradation of diuron [27].

Table2.4 Summary of type of bacteria used for biodegradation.

Conditions	Type of bacteria	Ref.
Biodegradation of diuron		
Anaerobic condition	-	
Aerobic condition	Sphingomonas sp.	[28]
Biodegradation of 3,4-dichloroaniline		
Anaerobic condition	Rhodococcus strain	[29]
Aerobic condition	Pseudomonas fluorescens 26-K	[30]

2.3.3 Photocatalytic degradation

The photocatalytic degradation is a common technique which is used to remove diuron from wastewater [31]. The catalysts is semiconductor materials such as TiO_2, SnO_2, Si, ZnO, WO_3, CdS, ZnS, $SrTiO_3$, WSe_2, Fe_2O_3, etc.[32] The photocatalysis can be divided 2 types that is homogenous and heterogeneous. This degradation uses UV lamp to generated UV light. The structure of intermedate products are investigated by gas chromatography mass spectrometry (GC-MS) which are shown in Table 2.5. And the degradation mechanism can be found in Figure 2.5.
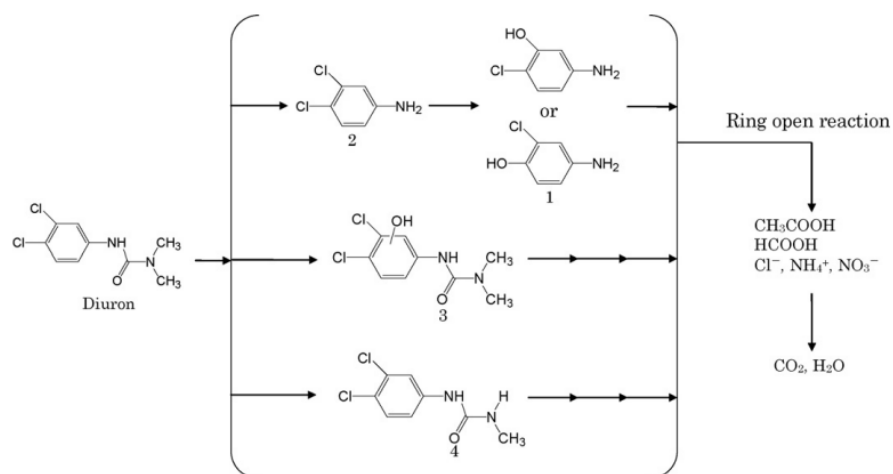
Figure 2.5 Photocatalytic degradation mechanism of diuron [31].

Table 2.5 The intermediate products by GC/MS in the photocatalytic degradation of diuron [31].

Product no.	R_t (min)	M.W.	Characteristic ions (m/z)	Compound
1	17.3	143	143, 71, 89	
2	19.3	161	161, 90, 80	
Diuron	33.6	232	232, 187, 72	
3	35.0	248	248, 218, 71	
4	40.3	218	218, 161, 71	

2.3.4 Electro-Fenton process

The electro-Fenton is a common method for degradation of organic pollutants in water. This method is very efficient system. It is based on the action of hydroxyl radicals that is produced by the Fenton's reagent (ferrous sulfate). Pt and carbon felt are utilized as cathode and anode, respectively [34]. The electrochemical oxidation reaction corresponding to the mineralization process and can be written the reaction as follow, equation 2.11. The structure of intermediate products are investigated by the liquid chromatography mass spectrometry (LC-MS) which are shown in Table 2.5.
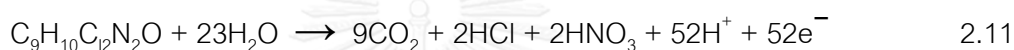
$$C_9H_{10}C_{l2}N_2O + 23H_2O \longrightarrow 9CO_2 + 2HCl + 2HNO_3 + 52H^+ + 52e^- \qquad 2.11$$

Table 2.6 The intermediate products by LC/MS in the electro-Fenton degradation of diuron [34].
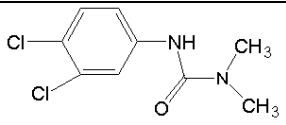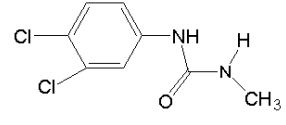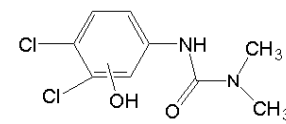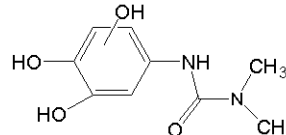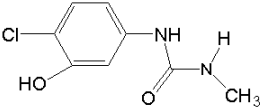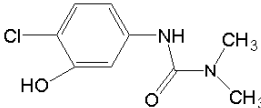
Compound	t_r^a (min)	$[M-H]^{+b}$	Identification	Chemical Structure
1	14.19	233	3-(3,4-Dichlorophenyl)-1,1-dimethyl urea (diuron)	
2	12.70	219	3-(3,4-Dichlorophenyl)-1,1-methyl urea	
3	9.78	249	3-(3,4-Dichloro-hydroxyphenyl)-1,1-dimethyl urea[c]	
4	3.08	213	3-(Trihydroxyphenyl)-1,1-dimethyl urea[c]	

Table 2.6 The intermediate products by LC/MS in the electro-Fenton degradation of diuron [34] (Conts.).

Compound	t_r^a (min)	$[M-H]^{+b}$	Identification	Chemical Structure
5	2.84	201	3-(3-Hydroxy-4-chlorophenyl)-1,1-methyl urea[d]	
6	2.33	215	3-(3-Hydroxy-4-chlorophenyl)-1,1-dimethyl urea[d]	

a t_r: retention time.

b Molecular weight of the corresponding molecular ion.

c For these degradation products, the position of hydroxyl group(s) on the aromatic ring or on the side methyl group cannot be attributed with certainty by the LC–MS method, and several position isomeric structures are compatible with the molecular weight of the molecular ion.

d For these degradation products, the position of the hydroxyl group on the aromatic ring has been deduced from the simultaneous dehalogenation/hydroxylation occurring during the diuron degradation.

The diuron degradation pathway from electro-fenton process was shown in Figure 2.6. The diuron (compound 1) was attacked by hydroxyl radical ($^\cdot$OH) and occurred the intermediated compounds as followed: (3,[3,4-dichlorohydroxyphenyl]-1,1-methylurea (compound 2), 3,[3-hydroxy 4-chlorohydroxyphenyl]-1,1-methylurea (compound 3), 3-[trihydroxyphenyl]-1,1-dimethylurea (compound 4), 3,[3-hydoxy-4-chlorophenyl]-1,1-methylurea (compound 5), and 3,[3-hydroxy-4-chlorophenyl]-1,1-dimethylurea (compound 6) were identified by LC–MS. In addition, dichloroaniline (compound 7), was identified by HPLC. The pathway can be divided 2 main routes as hydroxylation and dehydrogenation.
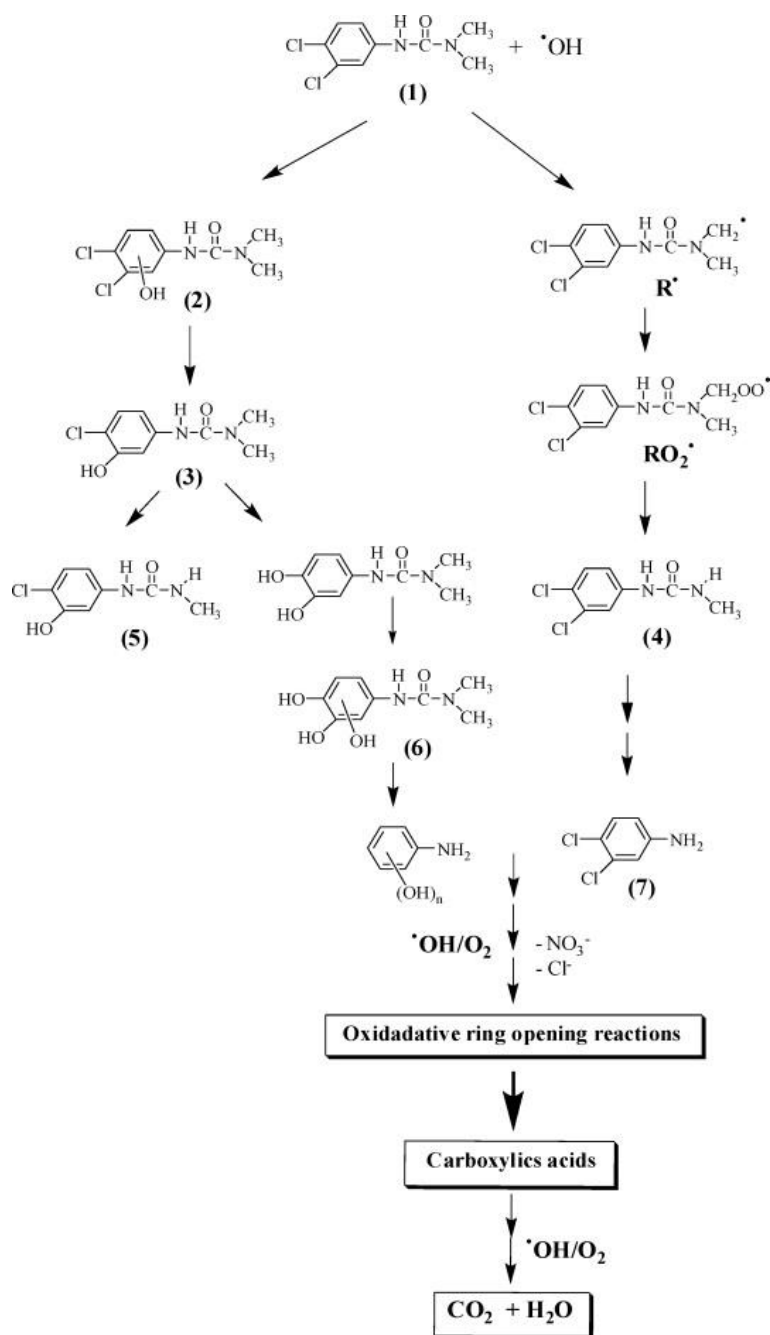
Figure 2.6 Degradation pathway for diuron mineralization by $^{\bullet}OH$ generated from electro-Fenton process [35].

CHAPTER III

EXPERIMENTAL METHODOLOGY

This chapter explains the detail of degradation process and can divide in 5 mainly sections that consist of chemicals, equipment, apparatus, experiment procedures, and analytical method.

3.1 Chemicals

The diuron was prepared from diuron (HPLC grade; 99.6 %, Sigma-Aldrich, Germany) and the deionized distilled water (resistivity 18 mΩ cm). The electrolyte including sodium sulfate (UNIVAR, USA), sodium chloride (UNIVAR, USA), sodium nitrate (UNIVAR, USA) and sodium hydrogen carbonate (UNIVAR, USA) were used for increasing electrical current. Sulfuric acid (98%, QReC, New Zealand), and sodium hydroxide (98%, Loba Chemie, India) were used to adjust the pH. Furthermore, acetonitrile (HPLC grade; 99.9, RCI Labscan, Thailand) was used as the mobile phase for analyzing diuron concentrations via high performance liquid chromatography (HPLC). Moreover, sodium hydroxide, potassium iodide (Kanto chemical, Japan), and ammonium molybdate (UNIVAR, USA) were a reagent A and potassium hydrogen phthalate (UNIVAR, USA) was a reagent B. In addition, the reagent A and B were used for analyzing hydrogen peroxide concentration via ultraviolet-visible spectroscopy (UV-vis). All of chemicals were the analytical grade.

3.2 Equipment

3.2.1 DC power supply

3.2.2 Ammeter

3.2.3 Voltmeter

3.2.4 Cellulose Acetate syringe filter with pore size 0.45 μm

3.2.5 Hot plate

3.3 Apparatus

The electrode materials were a titanium plate as the cathode and a graphite sheet as the anode. They immersed in diuron aqueous solution which was stirred by hot plate. DC power supply connected in series with ammeter and electrode, respectively. Voltmeter connected with electrode. The schematic diagram of experimental setup is shown in figure 3.1 and figure 3.2.
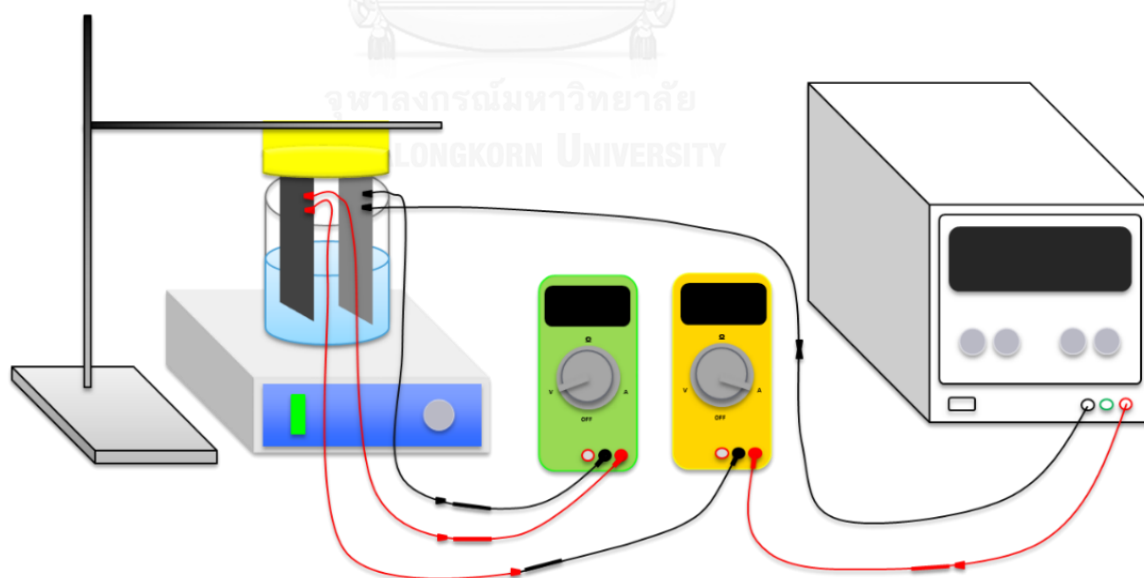
Figure 3.1 Schematic diagram of the experimental setup.

Figure 3.2 Photograph of the experimental setup.

3.4 Experimental procedures

Diuron aqueous solution was degraded by using the electrochemical advance oxidation process (EAOP). The initial diuron concentration was 10 ppm. The electrodes immersed in 550 ml of solution. This system had a low current density, so the electrolyte was added to increase current density. After that, the solution was stirred by the hot plate. Then, opened the DC power supply and adjusted until the electric current showed on the ammeter as 0.05 A. Finally, the samples were collected to analyze. For HPLC analyzer, sampling of 1 ml of volume was collected every hour until 6 hours. And for toc analyzer, sampling of 20 ml was collected every hour until 6 hours. For UV-vis, sampling of 1 ml of volume were collected every hour until 6 hours.

Table 3.1 List of experimental parameters.

Parameters	Details
The mixing speed (rpm)	800, 1,000, 1,200, and 1,500
The type of electrolyte	Na_2SO_4, NaCl, $NaNO_3$, and $NaHCO_3$
The applied electric current (mA)	30, 50, and 100
The initial pH of solution by adding Na2SO4 and NaOH	4, 7, and 11
The type of anode	Non-active (Graphite, Gold plated stainless steel) and Active (Stainless steel).
The temperature (°C)	10, 30, and 60.
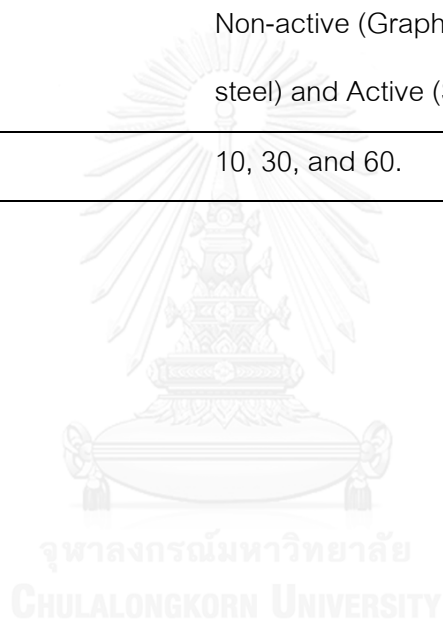
3.5 Analytical methods

3.5.1 High-Performance Liquid Chromatography (HPLC)

The samples that were filtrated through 0.45 µm of cellulose acetate syringe filter before being analyzed by high-performance liquid chromatography (LC-10A, Shimadzu) which is equipped with C18 column (phenomenex, Luna 5µ, 250 x 4.6 mm) and multiple wavelength UV diode array detector consisting of 240 nm, 250 nm, and 254 nm. The mobile phase are 70% (v/v) of acetonitrile and 30% (v/v) of deionized water. The total flow rate is 1.5 mL·min^{-1}. The retention time is 6 minutes. The column temperature is 60 °C. The injection volume is 20 µL with auto injection sampling. The photograph of HPLC is showed in Figure 3.3.

Figure 3.3 Photograph of High-Performance Liquid Chromatography (HPLC).

3.5.2 Total Organic Carbon Analyzer (TOC)

Amount of carbon in an organic carbon is identified by total organic carbon analyzer (TOC-VCPH, Shimadzu). This technique measures both a total carbon (TC) and an inorganic carbon [27]. Before analysis, sample solution are bubbled with nitrogen gas (HP grade, 99.995 %) for 20 minutes. The photograph of TOC removal is showed in Figure 3.4.

Figure 3.4 Photograph of Total Organic Carbon Analyzer (TOC).

3.5.4. Ultraviolet-Visible Spectrophotometer (UV-Vis)

Hydrogen peroxide (H_2O_2) is investigated by ultraviolet-visible spectrophotometer (UV-1700, Shimadzu). Hydrogen peroxide is used to confirm formation of hydroxyl radical ($OH^{\cdot}$). The photograph of UV-Visible spectrophotometer is showed in Figure 3.5. The procedure of H_2O_2 measurement was shown as followed:

1. Mixed 1 ml of the sample, 1 ml of A reagent, and 1 ml of B reagent.

2. The H_2O_2 is detected in wavelength at 350 nanometers.
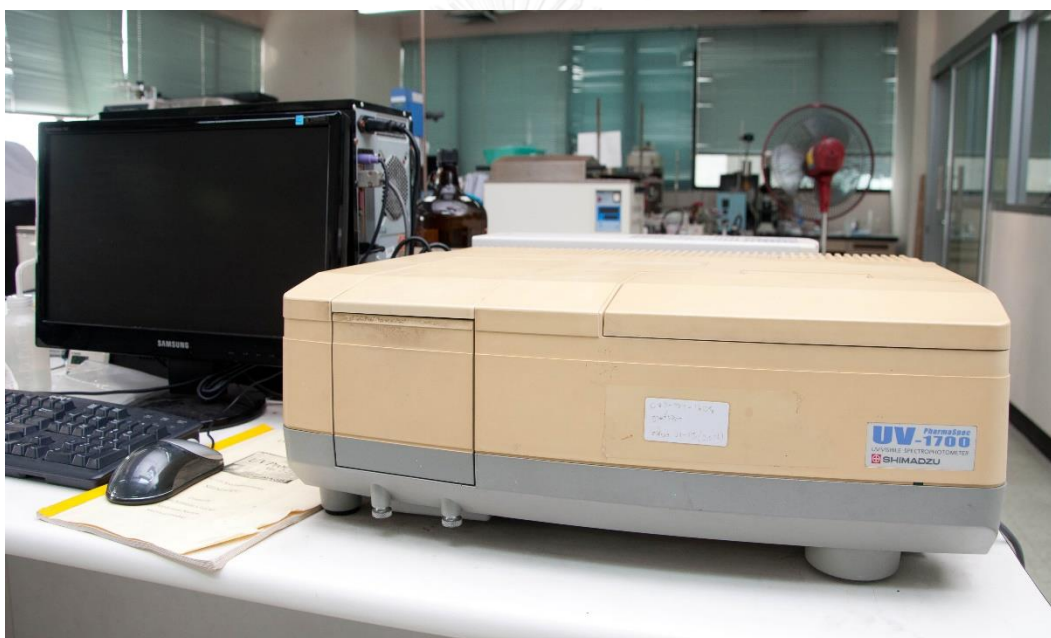
Figure 3.5 Photograph of Ultraviolet-Visible Spectrometry (UV-vis).

3.5.5 pH meter

The pH meter (Mettler toledo) is used to measure pH value of solution during the experiment. The probe can detect pH in range 0 to 14. The photograph of pH meter is showed in Figure 3.6.

Figure 3.6 Photograph of pH meter.

3.5.6 Conductivity meter

The conductivity meter (Mettler toledo) is used to measure conductivity value of solution during the experiment. The conductivity probe (Inlab®731, Mettler toledo) can detect in range 0.01 to 1,000 mS·cm^{-1}. The photograph of conductivity meter is showed in Figure 3.7.

Figure 3.7 Photograph of conductivity meter.

CHAPTER IV

RESULT AND DISCUSSION

This chapter describes all of the results and discussion which can be divided in 7 parts, i.e. characteristic of diuron degradation via EAOP, influence of mixing speed, type of electrolyte, applied electric current, initial pH value, type of electrode, and temperature.

4.1 Characteristic of diuron degradation

The electrochemical advanced oxidation process (EAOP) was used to removal diuron. When electric current is applied to the system, the diuron degradation starts. Hydroxyl radicals ($^{\bullet}OH$) were formed from water oxidation at the anode surface as shown in equation 4.1 [21]. The hydroxyl radicals have a short lifetime and cannot be detected, but the hydroxyl radicals can form to hydrogen peroxides (H_2O_2) as shown in Figure 4.2 [21]. Hydrogen peroxides can be detected in the solution, so they used to confirm hydroxyl radicals formation.

$$H_2O \rightarrow {}^{\bullet}OH + H^+ + e^- \qquad\qquad 4.1$$

$$^{\bullet}OH + {}^{\bullet}OH \rightarrow H_2O_2 \qquad\qquad 4.2$$

In these experiments, the applied current density was rather low, i.e. below 5 mA·cm^{-2}, so the corrosion of the graphite was small and did not affect amount of hydrogen peroxide that measured via colorimetric method [36]. The sampling solution was added with sodium carbonate (Na_2CO_3) which was the hydrogen peroxide scavenger

[36]. Adding sodium carbonate was used to investigate hydrogen peroxide formation. Table 4.1 shows the amount of hydrogen peroxide (H_2O_2) in deionized water before and after adding sodium carbonate.

Table 4.1 The amount of hydrogen peroxide (H_2O_2) in deionized water before and after adding sodium carbonate (Na_2CO_3).

Time	H_2O_2 concentration before adding Na_2CO_3 (ppm)	H_2O_2 concentration after adding Na_2CO_3 (ppm)
0	0.041	0.045
360	0.420	0.045

The deionized water was used instead of diuron at 50 mA of applied electric current, 0.05 mol·L^{-1} of sodium sulfate (Na_2SO_4) and 1,200 rpm of mixing speed. After 360 minutes, the hydrogen peroxide concentration in deionized water was 0.42 ppm. For diuron, the hydrogen peroxide concentration was 0.351 ppm. It is noted that hydroxyl radicals were recombined with hydrogen peroxides and destroyed diuron via hydroxylation, dehydrogenation, demethylation or dehalogenation [2, 14]. Therefore, diuron degradation takes place as shown in equation 4.3. The schematic diagram of mechanism of diuron degradation via electrochemical advanced oxidation process (EAOP) was shown in Figure 4.1.

$$\text{Diuron} + {}^{\bullet}\text{OH} \rightarrow \text{Diuron minerization products} \qquad 4.3$$
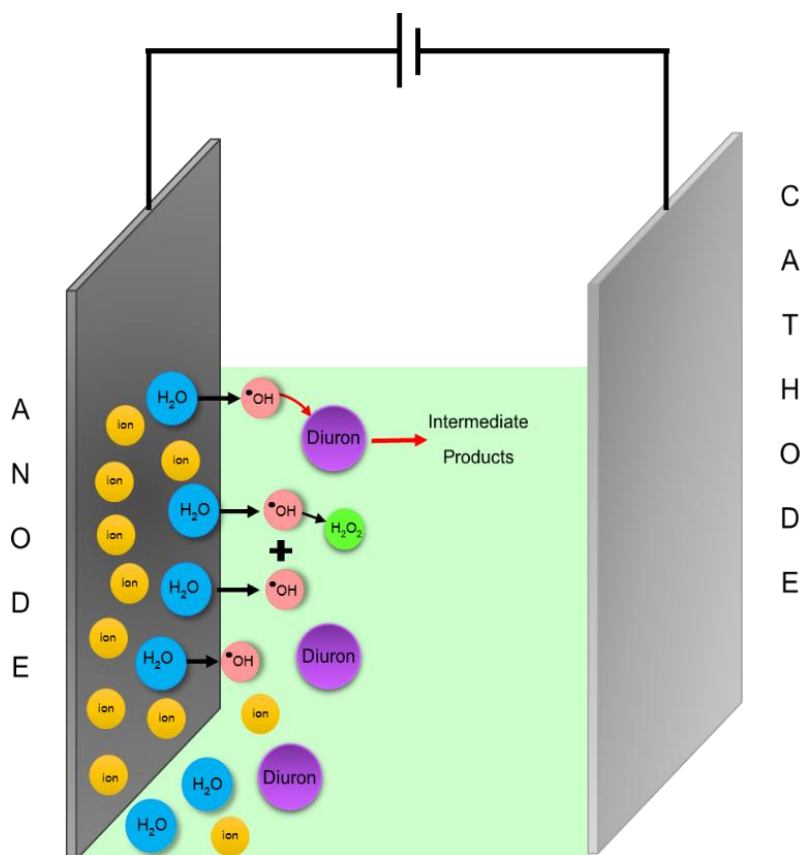
Figure 4.1 Schematic diagram of mechanism of diuron degradation via EAOP.

Moreover, hydroxyl radicals ($^\bullet$OH) could combine with hydrogen peroxides (H_2O_2) to hydroperoxyl radical ($HO_2^\bullet$) as followed in equation 4.4 and 4.5 [37]. Hydrogen peroxides and hydroperoxyl radical were weak oxidants, but hydroxyl radicals were powerful oxidants.

$$H_2O_2 + {}^\bullet OH \rightarrow HO_2^\bullet + H_2O \qquad\qquad 4.4$$

$$HO_2^\bullet + {}^\bullet OH \rightarrow H_2O + O_2 \qquad\qquad 4.5$$

Increasing experiment time results the concentration of hydrogen peroxide (H_2O_2) increases as shown in Figure 4.2. This implies that hydroxyl radicals are generated in this system. As result, the diuron degradation increases with increased time because it is exposed to the reactive species for long period of time. The concentration of diuron decreased with time as shown in Figure 4.3. After 60 minutes, diuron concentration decreased rapidly as more than 50%. At 360 minutes, the diuron can be degraded more 98% due to diuron were mineralized by hydroxyl radicals ($^\bullet$OH).
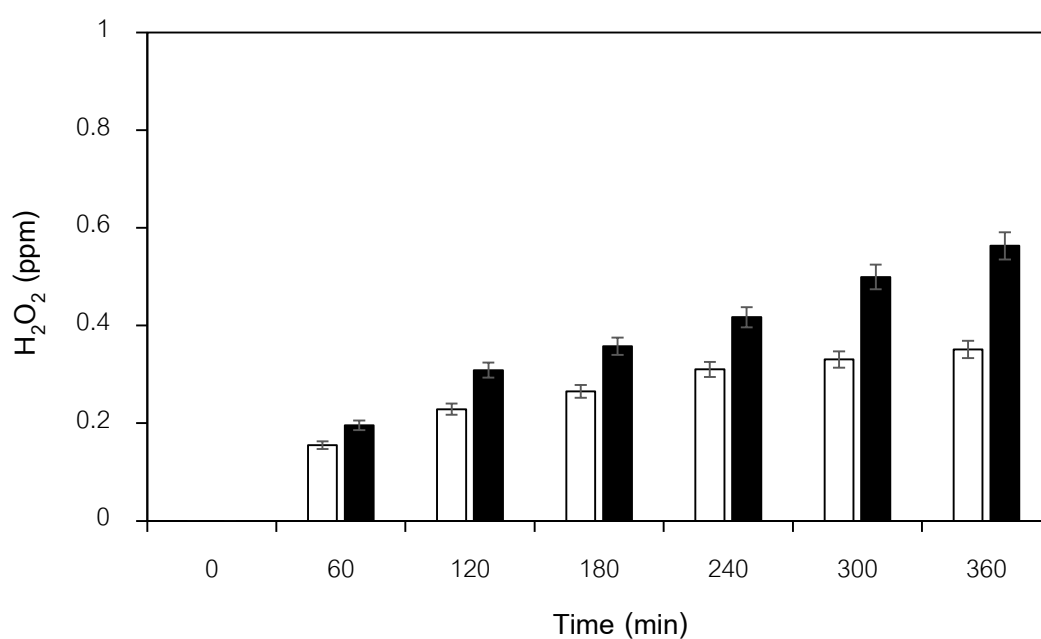
Figure 4.2 Hydrogen peroxide concentration (H_2O_2) at 50 mA, 0.05 mol·L^{-1} of Na_2SO_4, and 1,200 rpm; ($\square$) in 10 ppm of diuron and ($\blacksquare$) in deionized water.
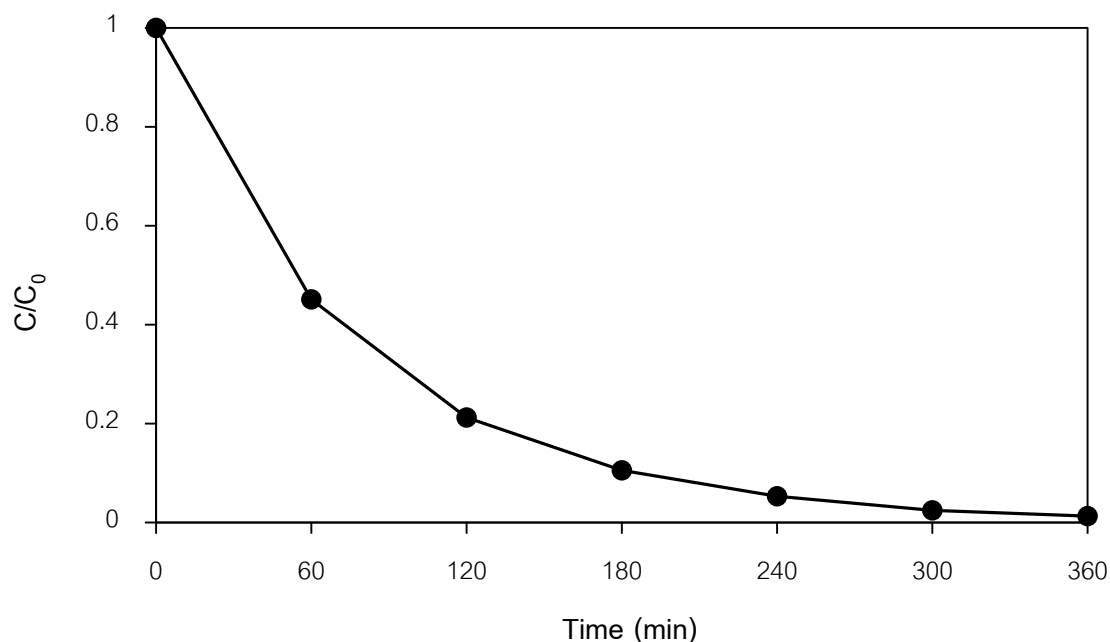
Figure 4.3 Diuron degradation via EAOP at 50 mA, 0.05 mol·L^{-1} of Na$_2$SO$_4$, and 1,200 rpm during 6 hours.

The ratio of diuron and hydroxyl radical was 1:4. The calculation of ration diuron and hydroxyl radical were showed in Appendix E. Therefore, the hydroxyl radicals were excessed when comparing with diuron as a result rate of reaction depended on diuron concentration. The degradation of diuron via electrochemical advanced oxidation process (EAOP) was described by pseudo-first-order kinetic as presented in equation 4.5 and 4.6:

$$-r = \frac{dC}{dt} = k_{app}C \qquad\qquad 4.5$$

$$\ln\left(\frac{C_0}{C}\right) = k_{app}t \qquad\qquad 4.6$$

where C is the concentration of diuron be degraded (ppm), C$_0$ is the initial diuron concentration (ppm), r is the rate of diuron degradation, k$_{app}$ is the apparent rate constant (min^{-1}), and t is the operating time [33], respectively. The kinetic constant of diuron

degradation is 1.25×10^{-2} min^{-1} with $R^2 > 0.9$. Figure 4.4 shows kinetic plot of diuron degradation.
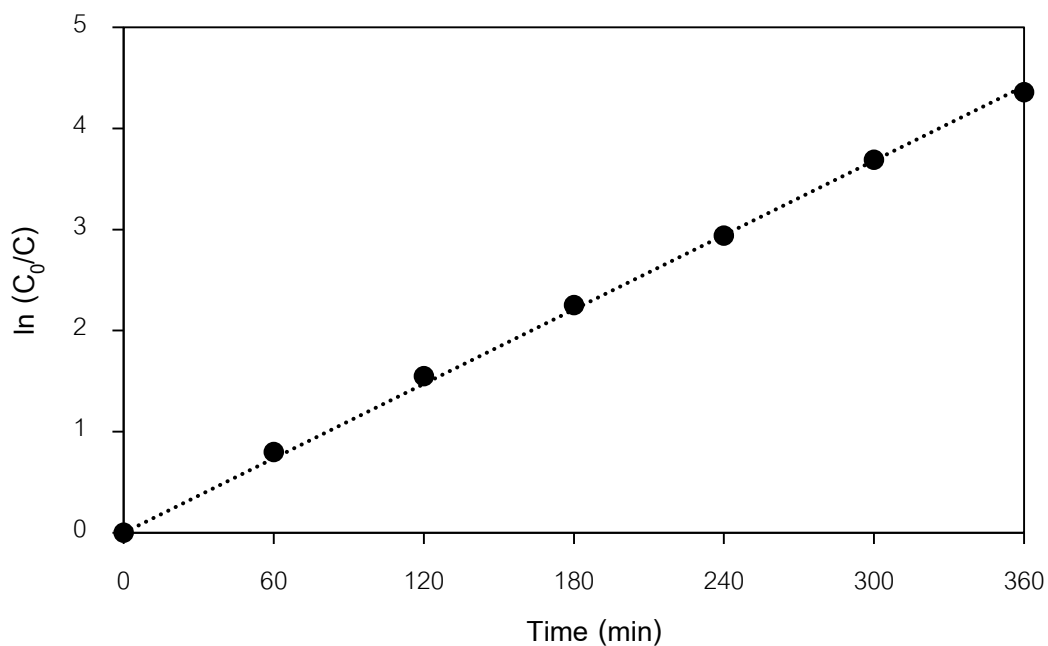
Figure 4.4 The kinetic plot of diuron degradation via EAOP at 50 mA, 0.05 mol·L^{-1} of Na$_2$SO$_4$, and 1,200 rpm during 6 hours.

While the diuron was degraded, the total organic carbon (TOC) of solution decreased. Although the TOC decreased, it was small as compared with decreasing concentration of diuron. At 360 minutes, efficiency of diuron degradation and TOC removal were about 98% and 35%, respectively, at 50 mA of applied electric current and 0.05 mol·L^{-1} of Na$_2$SO$_4$. It is noted that intermediate products are formed through diuron degradation. The mineralization current efficiency (MCE) was presented in equation 4.7 [38, 39]:

$$\text{MCE (\%)} = \frac{nFV_s\Delta(TOC)_{exp}}{4.32\times10^7 mIt} \times 100 \qquad 4.7$$

where F is the Faraday constant (96,487 $C \cdot mol^{-1}$), V_s is the solution volume (L), $\Delta(TOC)_{exp}$ is the experimental TOC decay ($mg \cdot L^{-1}$), I is the applied current (A), t is the operating time (h), 4.32×10^7 is the conversion factor (3,600 $s \cdot h^{-1}$ × 1,200 $mg \cdot mol^{-1}$), m is the number of carbon atoms of diuron (9 C atoms), and E_{cell} is the applied potential (V). The number of electrons consumed per diuron molecule (n) was taken as 36 for the complete mineralization to carbon dioxides (CO_2), chloride ions (Cl^-), and ammonium ions (NH_4^+), as followed in equation 4.8:

$$C_9H_{10}Cl_2N_2O + 17H_2O \rightarrow 9\ CO_2 + 2\ Cl^- + 2NH_4^+ + 36H^+ + 36e^- \qquad 4.8$$
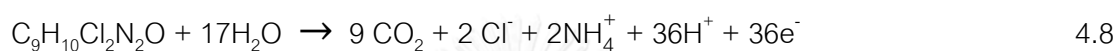
For degradation of diuron at 50 mA of applied electric current and 0.05 $mol \cdot L^{-1}$ of Na_2SO_4, the mineralization current efficiency was 3.29% and 2.58% at 60 minutes and 360 minutes. The result is indicated that the mineralization current efficiency decreased with time [40].
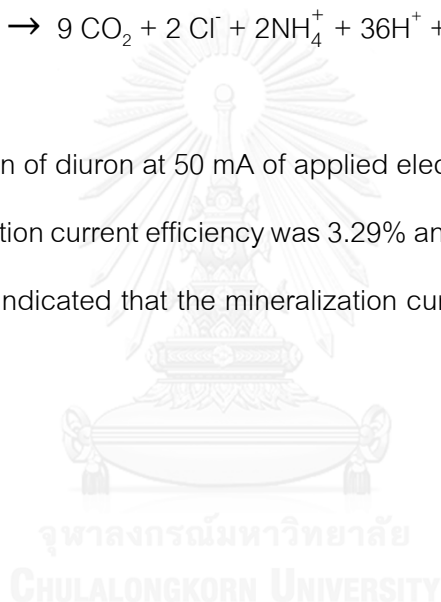
4.2 Influence of mixing speed.

The influence of mixing speed was the first parameter that is studied by varying the mixing speed to 800 rpm, 1,000 rpm, 1,200 rpm, and 1,500 rpm, respectively, at 50 mA of the applied electric current, 0.05 mol·L^{-1} of sodium sulfate (Na_2SO_4), and neutral initial solution (pH 7).

Figure 4.5 indicates the degradation of diuron increased when the mixing speed increased. At 360 minutes, the percentage of diuron degradation is 93.75, 96.02, 98.72, and 99.2 when the mixing speed is 800 rpm, 1,000 rpm, 1,200 rpm, and 1,500 rpm, respectively. It is noted that the speed at 1,200 rpm and 1,500 rpm, the efficiency of diuron degradation is not significantly affected by mixing speed. Therefore, this system is negligible the influence of mass transfer resistant when using speed exceed 1,200 rpm.
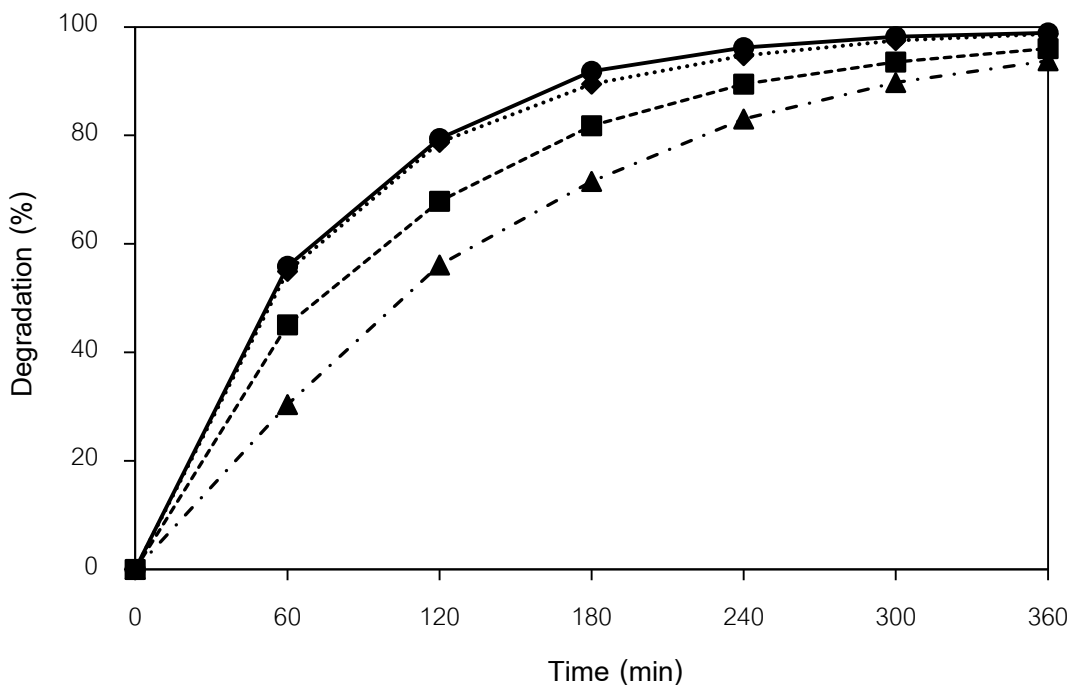
Figure 4.5 Influence of mixing speed for the diuron degradation via EAOP: (▲) 800 rpm, (■) 1,000 rpm, (◆) 1,200 rpm, and (●) 1,500 rpm.

The apparent rate constant increased with mixing speed due to influence of mass transfer. The apparent rate constant is 7.5×10^{-2} min^{-1} (R^2 = 0.995), 9.2×10^{-2} min^{-1} (R^2 = 0.998), 1.25×10^{-2} min^{-1} (R^2 = 0.997) and 1.32×10^{-2} min^{-1} (R^2 = 0.996) when the mixing speed is 800 rpm, 1,000 rpm, 1,200 rpm, and 1,500 rpm, respectively. The reaction is fitted in psudo-first-order kinetic. The data was listed in Table 4.2.

Table 4.2 Data of the apparent rate constant (k_{app}) on the influence of mixing speed.

Mixing speed (rpm)	The apparent rate constant (min^{-1})	R^2
800	7.5×10^{-2}	0.995
1,000	9.2×10^{-2}	0.998
1,200	1.25×10^{-2}	0.997
1,500	1.32×10^{-2}	0.996

4.3 Influence of electrolyte type.

The type of electrolytes was an important parameter. Electrolytes helped for increasing conductivity and decreasing resistance [24]. In this experiment, sodium sulfate (Na_2SO_4), sodium chloride (NaCl), sodium nitrate ($NaNO_3$) and sodium hydrogen carbonate ($NaHCO_3$) were selected for using in this study at 50 mA of applied electric current, neutral initial solution (pH 7), and 1,200 rpm of mixing speed. All of the concentration of electrolytes were controlled as 0.05 mol·L^{-1}.

The efficiency of diuron degradation on the influence of electrolyte type is showed in Figure 4.6. At 360 minutes, the percentage of diuron removal is 99.78, 98.98, 98.72, and 98.49 when the electrolyte is NaCl, $NaNO_3$, Na_2SO_4, and $NaHCO_3$, respectively. When the solution is without the electrolyte, the efficiency of degradation is 14.33% due to current density is low and the conductivity is also lower than water oxidation.

Table 4.3 shows rate of reaction constant and the regression coefficients (R^2) on the influence of electrolyte type. As the results indicate that electrolytes play role in the system and affect the efficiency of degradation and rate of reaction. In these experiments, electrolytes had same cation as sodium ion (Na^+), but anions were different. From the results indicated that decreasing concentration of diuron was result from the influence of anion. The nature of electrolyte can highly affect the rate of reaction because some ions can consume hydroxyl radicals as a result to concentration of hydroxyl radicals decreased [37, 41] and changing concentration of hydrogen peroxide.
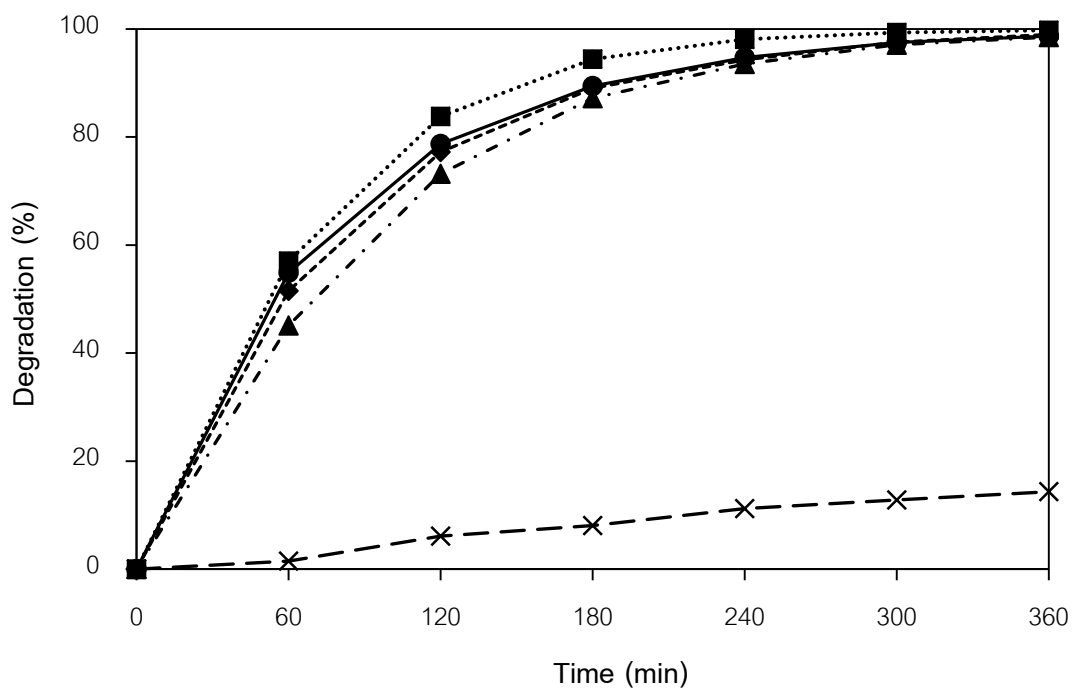
Figure 4.6 Influence of electrolyte for the diuron degradation via EAOP: (▲) $NaHCO_3$, (■) NaCl, (◆) $NaNO_3$, (●) $Na2_SO_4$, and (X) no electrolyte.

Table 4.3 Data of the apparent rate constant (k_{app}) on the influence of electrolyte type.

Type of electrolytes	The apparent rate constant (min^{-1})	R^2
No electrolyte	5×10^{-4}	0.981
NaCl	1.66×10^{-2}	0.997
$NaNO_3$	1.24×10^{-2}	0.998
Na_2SO_4	1.25×10^{-2}	0.997
$NaHCO_3$	1.16×10^{-2}	0.998

In addition, the oxidation of supported electrolytes can form the unwanted products on the anode surface. Some new oxidants can combine with the hydroxyl radicals ($^\bullet$OH). For chloride ion (Cl^-), chloride ions can be oxidized to chlorines (Cl_2) as shown in equation 4.9. The chlorines were transformed to hypochlorous acids (HClO) and then to hypochlorite (ClO^-) as presented in equation 4.10 and 4.11 [2, 15, 24]. Although the organochlorinated species were highly reactive with organic compound, they have toxicity to animals including human.

$$2\,Cl^- \rightarrow Cl_2 + 2e^- \qquad\qquad 4.9$$

$$Cl_2 + H_2O \rightarrow HClO + Cl^- + H^+ \qquad\qquad 4.10$$

$$HClO \leftrightarrow H^+ + ClO^- \qquad\qquad 4.11$$

For sulfate ion (SO_4^{2-}), sulfate ions were oxidized to persulfate ions ($S_2O_8^{2-}$), according to equation equation 4.12 [15, 42]:

$$2SO_4^{2-} \leftrightarrow S_2O_8^{2-} + 2e^- \qquad\qquad 4.12$$

For nitrate ion (NO_3^-), nitrate ions were reduced to nitrite ions (NO_2^-) and then to ammonias (NH_3) as shown in equation 4.13 and 4.14 [43]:

$$NO_3^- + H_2O + 2e^- \rightarrow NO_2^- + 2OH^- \qquad\qquad 4.13$$

$$NO_2^- + H_2O + 2e^- \rightarrow NH_3 + 8OH^- \qquad\qquad 4.14$$

For bicarbonate ion (HCO_3^-), the bicarbonate ions were decomposed to carbonate ion (CO_3^{2-}). The hydroxyl radicals ($^\bullet OH$) reacted with carbonate ion (CO_3^{2-}) and oxidized to peroxydicarbonate ions ($C_2O_6^{2-}$), according to equation 4.15 and 4.16 [44]:

$$HCO_3^- \leftrightarrow CO_3^{2-} + H^+ \qquad\qquad\qquad 4.15$$

$$2CO_3^{2-} + 2HO^\bullet \rightarrow C_2O_6^{2-} + 2H_2O \qquad\qquad\qquad 4.16$$
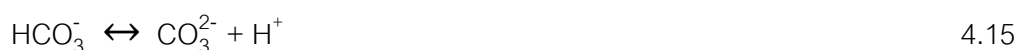
The diuron concentration decreased with time because of continuous generation of hydroxyl radicals. The hydroxyl radicals attacked diuron structure to the intermediated products. The hydrogen peroxides formation were representative of hydroxyl radicals. Therefore diuron degradation increased when formation of hydrogen peroxide increased except using $NaHCO_3$ as electrolyte (see in Figure 4.7). At Na_2SO_4 as electrolyte, amount of hydrogen peroxide slightly increased because hydrogen peroxide was consumed by $SO_4^{\bullet-}$ as shown in equation 4.17 and 4.18 [41].

$$SO_4^{2-} + {}^\bullet OH \rightarrow SO_4^{\bullet-} + OH^- \qquad\qquad\qquad 4.17$$

$$SO_4^{\bullet-} + H_2O_2 \rightarrow SO_4^{2-} + H^+ + HO_2^\bullet \qquad\qquad\qquad 4.18$$

Figure 4.8 shows efficiency of total organic carbon (TOC) removal at 360 minutes is about 35%, 40 %, 59%, and 60% when the electrolyte is Na_2SO_4, $NaNO_3$, $NaHCO_3$, and NaCl. Although the TOC removal at $NaHCO_3$ is higher than using Na_2SO_4 and $NaNO_3$ as electrolyte, the degraded efficiency is lowest due to bicarbonate (HCO_3^-) ions occur as carbonate ions (CO_3^{2-}). From results of TOC removal indicates this system cannot completely mineralization and forms intermediate products.
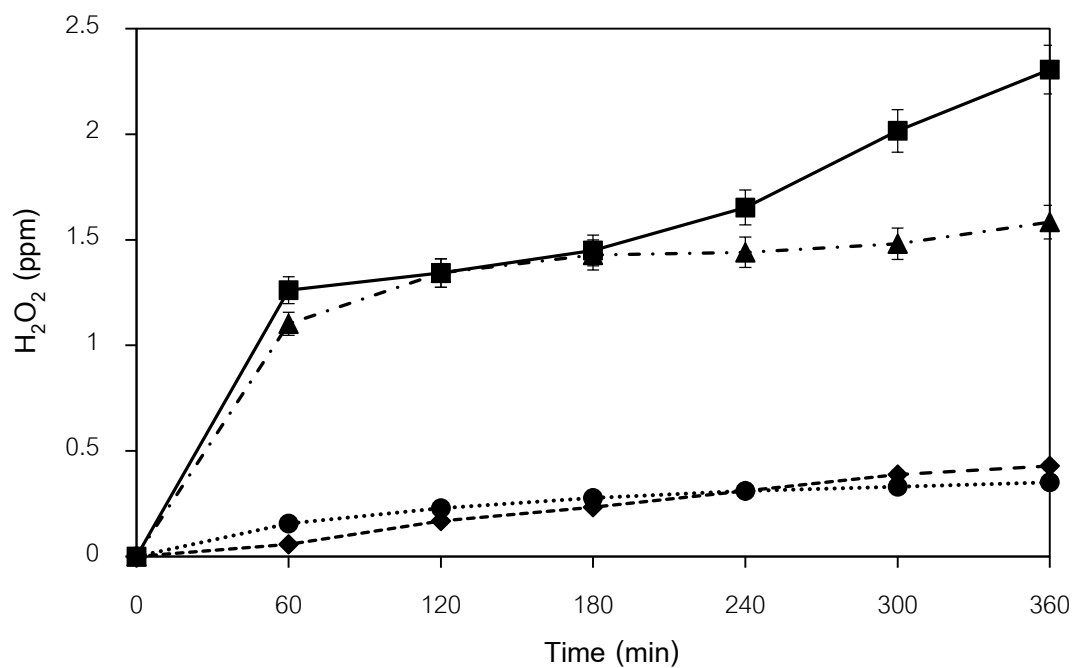
Figure 4.7 Hydrogen peroxide concentration in diuron on the influence of electrolyte for the diuron degradation via EAOP: (▲) $NaHCO_3$, (■) $NaCl$, (◆) $NaNO_3$ and (●) Na_2SO_4.
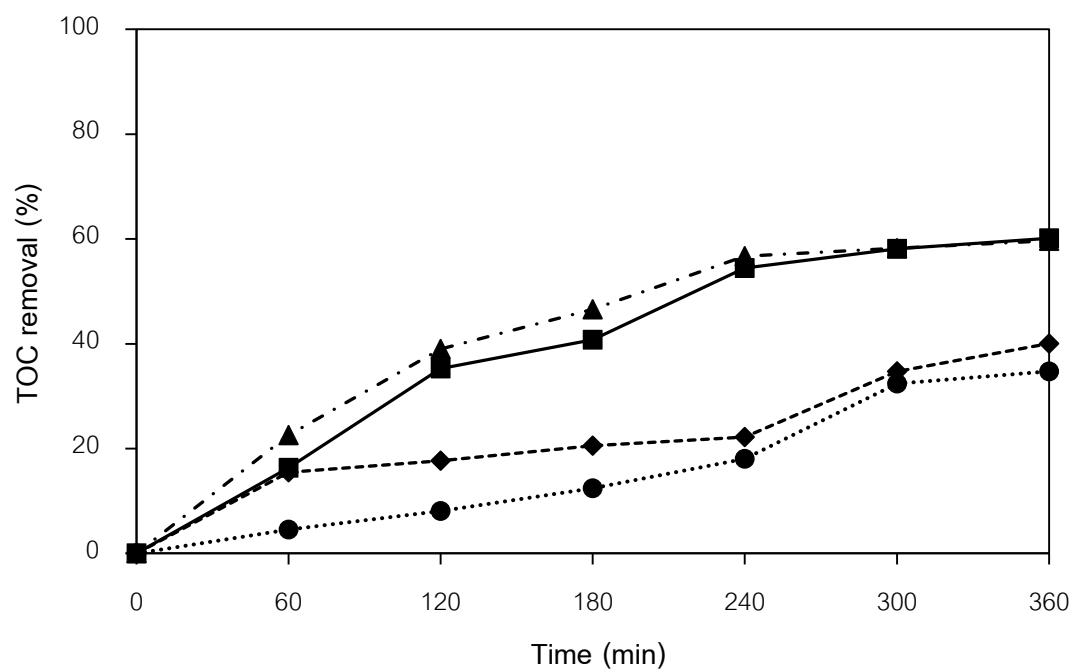
Figure 4.8 Total organic carbon on the influence of electrolyte for the diuron degradation via EAOP: (▲) $NaHCO_3$, (■) $NaCl$, (◆) $NaNO_3$ and (●) Na_2SO_4.

The degradation of diuron occurs intermediate products which detected by HPLC as seen in Figure 4.9 - 4.12. For sulfate ions (SO_4^{2-}) as shown in Figure 4.9, the intermediate products were found at the retention time (R_T) of 1.48, 1.75, 1.90, 1.99, 2.29, 2.61, and 2.88 minutes, respectively. For chloride ions (Cl^-) as shown in Figure 4.10, the intermediate products were found at the retention time (R_T) of 1.52, 1.99, 2.58, 2.75, 4.16, and 4.61 minutes, respectively. For nitrate ions (NO_3^-) as shown in Figure 4.11, the intermediate products were found at the retention time (R_T) of 2.00, 2.30, 2.56, and 2.98 minutes, respectively. For bicarbonate ions (HCO_3^-) as shown in Figure 4.12, the intermediate products were found at the retention time (R_T) of 1.35, 1.99, 2.29, 2.48, and 2.75 minutes, respectively.
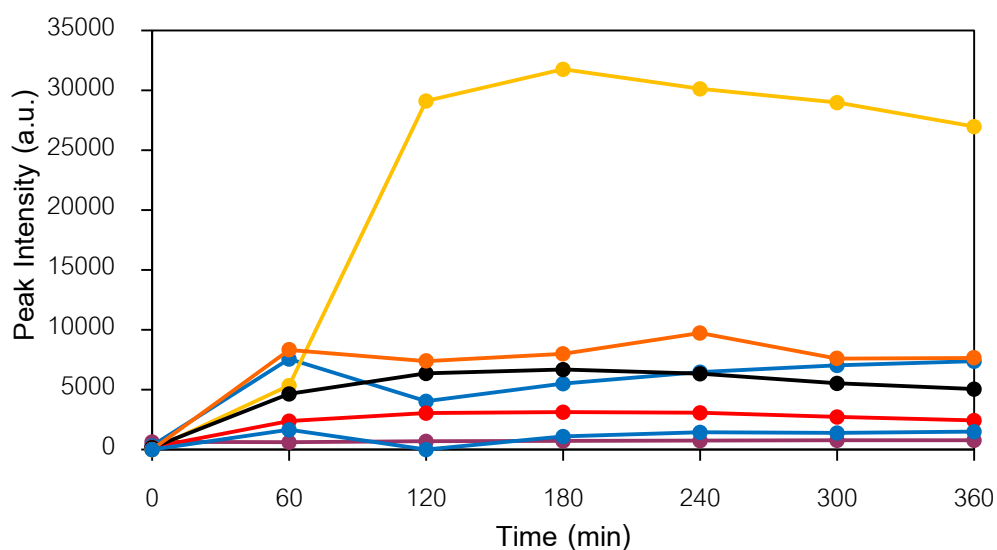
Figure 4.9 HPLC intermediate profile of diuron degradation via EAOP at sulfate (SO_4^{2-}) ion: (●) R_T = 1.48 min, (●) R_T = 1.75 min, (●) R_T = 1.90 min, (●) R_T = 1.99 min, (●) R_T = 2.29 min, (●) R_T = 2.61 min, and (●) R_T = 2.98 min.
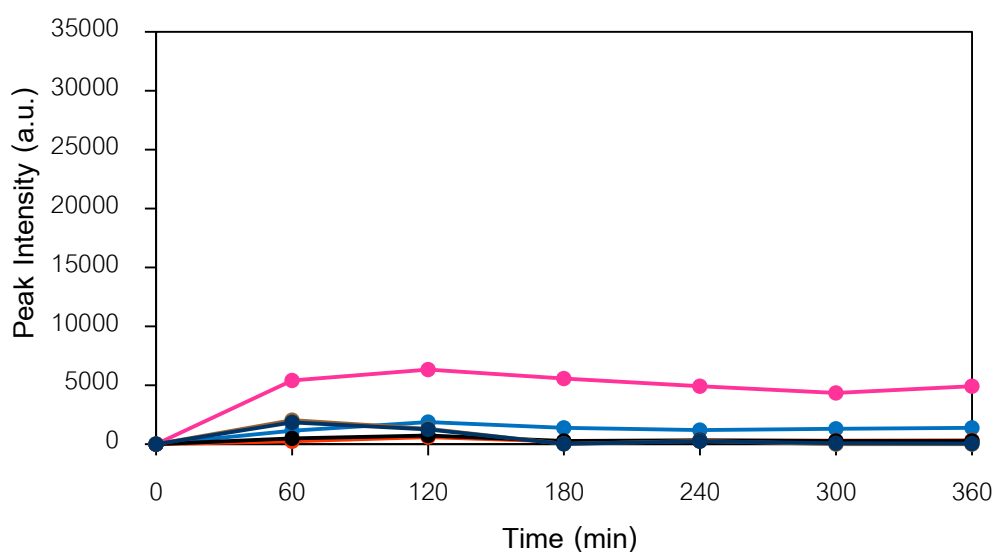
Figure 4.10 HPLC intermediate profile of diuron degradation via EAOP at chloride (Cl⁻) ion: ($\bullet$) R_T = 1.52 min, ($\bullet$) R_T = 1.99 min, ($\bullet$) R_T = 2.58 min, ($\bullet$) R_T = 2.75 min, ($\bullet$) R_T = 4.16 min, and ($\bullet$) R_T = 4.61 min.
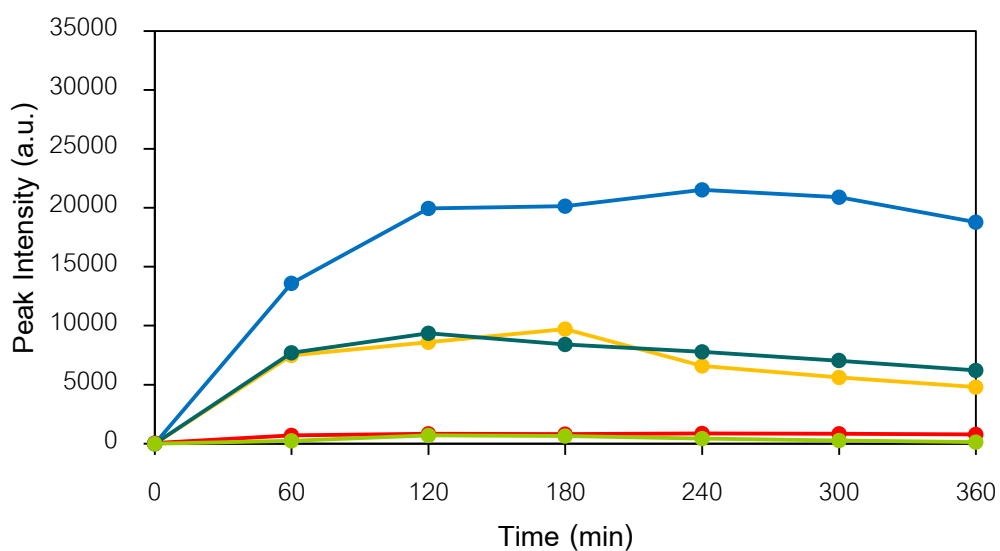
Figure 4.11 HPLC intermediate profile of diuron degradation via EAOP at nitrate (NO_3^-) ion: ($\bullet$) R_T = 2.00 min, ($\bullet$) R_T = 2.30 min, ($\bullet$) R_T = 2.56 min, ($\bullet$) R_T = 2.98 min, and ($\bullet$) R_T = 4.92 min.
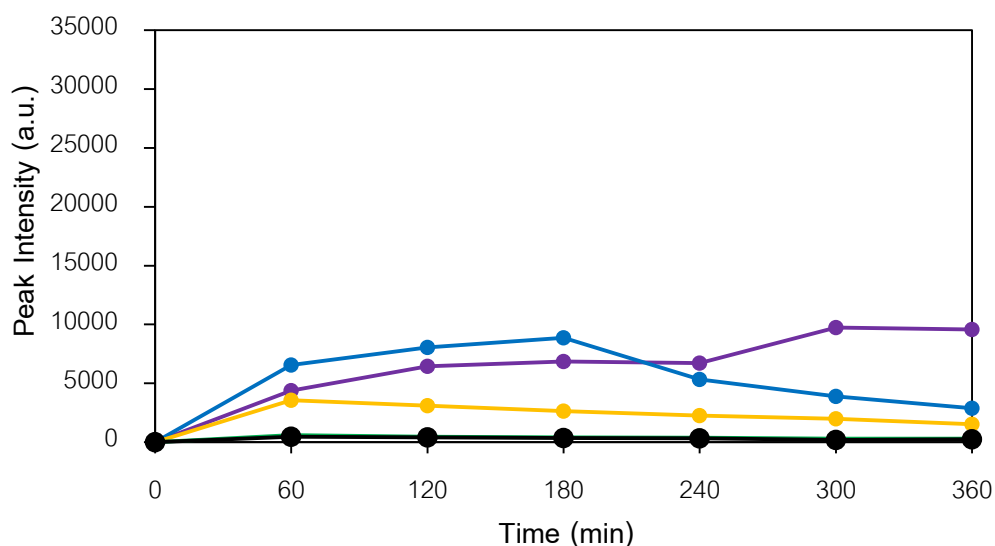
Figure 4.12 HPLC intermediate profile of diuron degradation via EAOP at bicarbonate (HCO_3^-) ion: (●) R_T = 1.35 min, (●) R_T = 1.99 min, (●) R_T = 2.29 min, (●) R_T = 2.48 min, and (●) R_T = 2.75 min.

In addition to the influence of anion affected to the efficiency of diuron degradation, it also involved to intermediate products formation. Some anions, i.e. nitrate ion (NO_3^-), chloride ion (Cl^-), participated in diuron degradation and caused different pathway [45]. Therefore, using difference anions were resulting to difference degradation pathway. The total toxicity of treated solution with sulfate and nitrate ions reduces when compared with the toxicity of pure diuron that was suggested by Khlongton, W [46].

4.4 Influence of applied electric current.

The applied electric current was one of the important variables that has influence of oxidation ability in EAOPs [13, 16, 17]. In this experiment, the influence of applied electric current was investigated by varying applied current to 30 mA, 50 mA, and 100 mA which corresponded to 1.33 mA/cm^2, 2.22 mA/cm^2, and 4.44 mA/cm^2, respectively, at 50 mA of applied electric current, 0.05 mol·L^{-1} of sodium sulfate (Na$_2$SO$_4$), and neutral initial solution (pH 7). At 360 minutes, the percentage of diuron degradation is 95.94, 98.72, and 99.16 when the applied electric current is 30 mA, 50 mA, and 100 mA, respectively (as seen in figure 4.13). Increasing applied electric current is significant to increasing of hydroxyl radical ($^•$OH) formation [47]. The formation of hydrogen peroxide also increases with increasing the applied electric current as shown in Figure 4.12.

Figure 4.13 Influence of applied electric current for the diuron degradation via EAOP: (▲) 30 mA, (●) 50 mA, and (■) 100 mA.

The value of apparent rate constants (k_{app}) and the regression coefficients (R^2) are presented in Table 4.4. In general, the rate of diuron degradation increased with increasing applied electric current for all EAOPs [41]. Therefore, the enhancement of applied density affects to increase apparent rate constant [37].

Table 4.4 Data of the apparent rate constant (k_{app}) on the influence of applied electric current.

Applied electric current (mA)	The apparent rate constant (min^{-1})	R^2
30	8.5×10^{-3}	0.990
50	1.25×10^{-2}	0.997
100	1.31×10^{-2}	0.995

Although the applied electric current increase from 50 mA to 100 mA, the degradation of diuron does not increase significantly. When the current is applied exceed 50 mA as a result to occur side reaction which is the competing radical to radical interaction [14, 17]. From Figure 4.14, amount of hydrogen peroxide increases with increasing the applied current. Even though the formation of H_2O_2 at 100 mA is more than 50 mA of applied electric current, the degradation of diuron is less different.

Although the diuron degraded almost 100% which is result from HPLC, the efficiency of total organic carbon (TOC) removal (shown in Figure 4.15) is just 26%, 35%, and 38% at 30 mA, 50 mA, and 100 mA, respectively, indicating that the oxidation process destroys diuron structure, but it cannot complete mineralize all the intermediates [16].
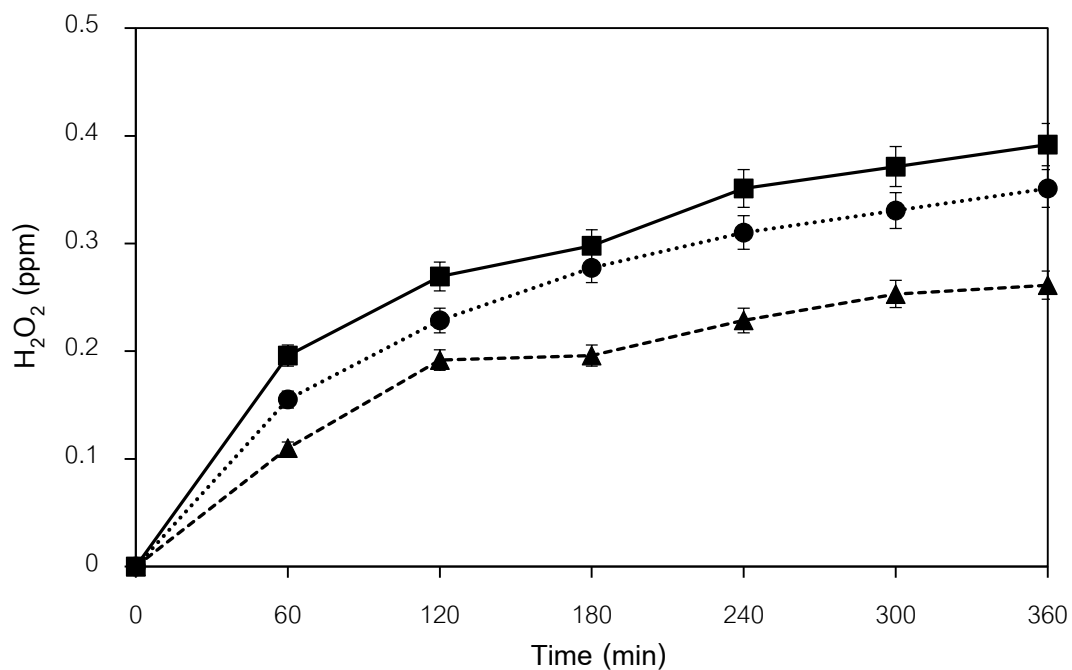
Figure 4.14 Hydrogen peroxide concentration in diuron on the influence of applied electric current for the diuron degradation via EAOP: (▲) 30 mA, (●) 50 mA, and (■) 100 mA.
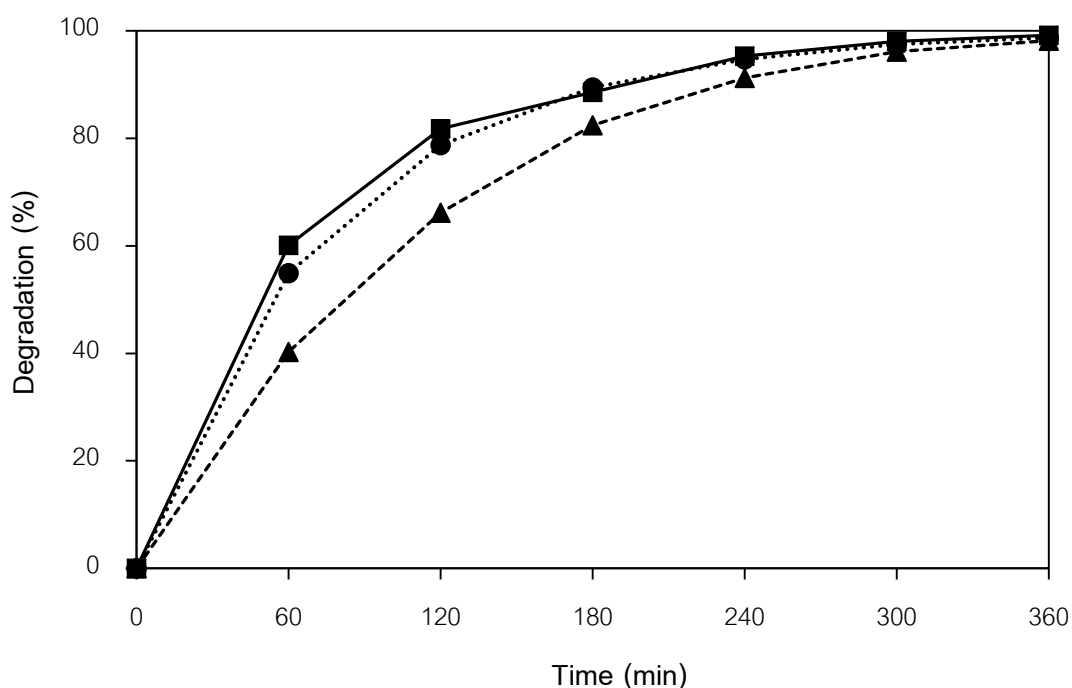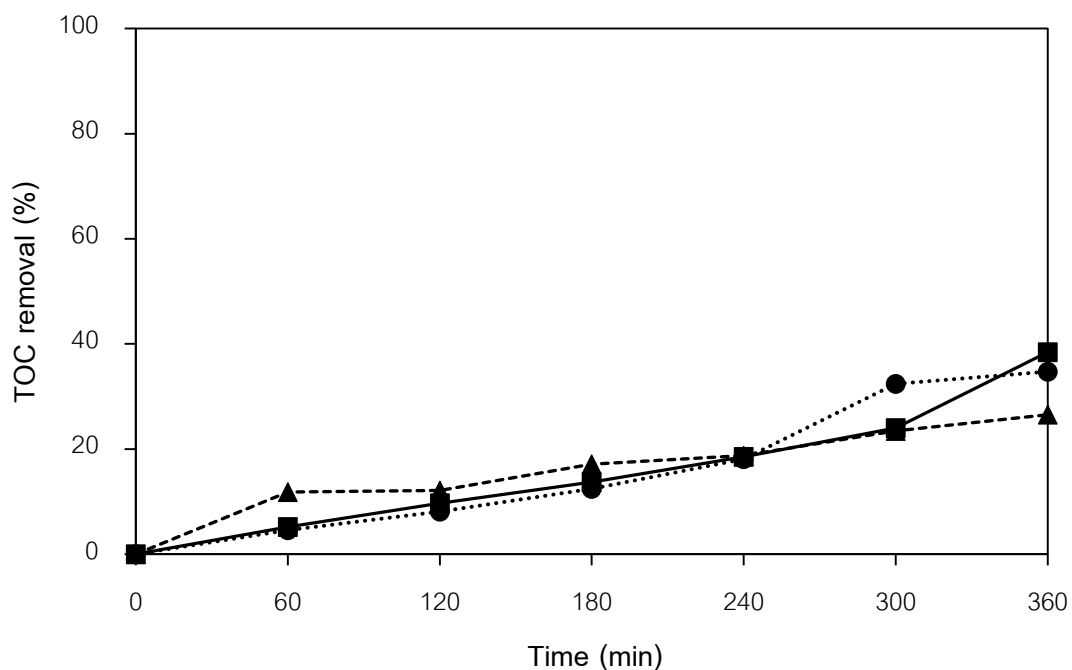

Figure 4.15 Total organic carbon on the influence of applied electric current for the diuron degradation via EAOP: (▲) 30 mA, (●) 50 mA, and (■) 100 mA.

The intermediate products were detected from HPLC. As results in Figure 4.16 and 4.17 show peak intensity with time on the influence of applied electric current. At 30 mA, six compounds were detected as shown in Figure 4.16. The intermediate products were found at the retention time (R_T) of 1.50, 1.60, 2.00, 2.30, 2.56, and 2.98 minutes, respectively.
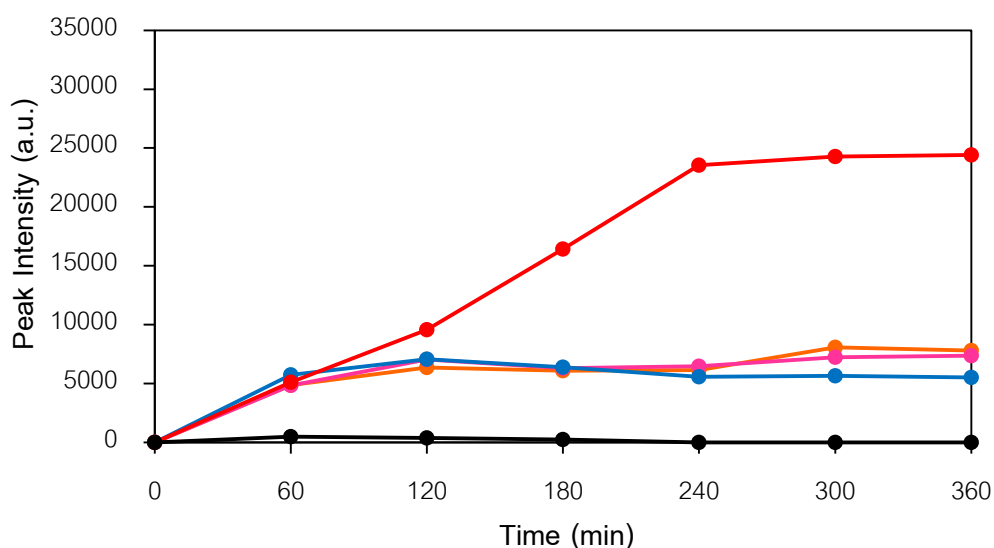
Figure 4.16 HPLC intermediate profile of diuron degradation via EAOP at 30 mA: (●) R_T = 1.50 min, (●) R_T = 1.60 min, (●) R_T = 2.00 min, (●) R_T = 2.30 min, (●) R_T = 2.56 min, and (●) R_T = 2.98 min.

Figure 4.17 shows intermediate profile with time when applied electric current is 100 mA. The intermediate products were found when at retention time (R_T) of 1.47, 1.90, 2.01, 2.09, 2.30, 2.57, and 2.96 minutes, respectively. At 50 mA as shown in Figure 4.9, the intermediate products were found at the retention time (R_T) of 1.48, 1.75, 1.90, 1.99, 2.29, 2.61, and 2.88 minutes, respectively. Results shown that increasing applied current induced to generate more hydroxyl radicals. Therefore, hydroxyl radicals can attack diuron as several poitions as a result different intermediate product formation.
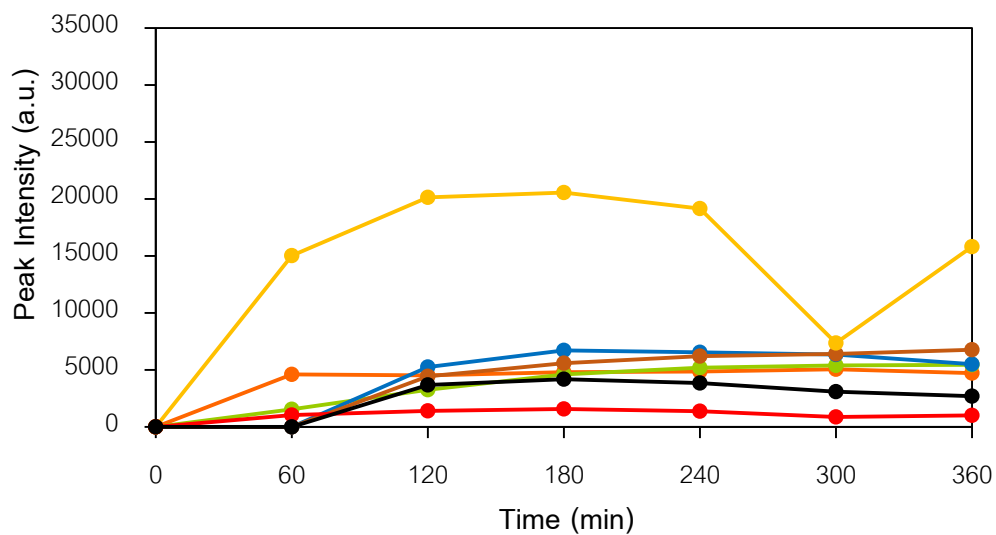
Figure 4.17 HPLC intermediate profile of diuron degradation via EAOP at 100 mA: (●) R_T = 1.47 min, (●) R_T = 1.90 min, (●) R_T = 2.01 min, (●) R_T = 2.09 min, (●) R_T = 2.30 min, (●) R_T = 2.57 min, and (●) R_T = 2.96 min.

4.5 The influence of initial pH

The influence of the initial pH on diuron degradation via EAOP is investigated by using sodium hydroxide (NaOH) and sulfuric acid (H_2SO_4) to adjust pH value in the range of 4-11 at 50 mA of applied electric current, 0.05 mol·L^{-1} of sodium sulfate (Na_2SO_4), and 1,200 of mixing speed. As the results in Figure 4.18 present the efficiency of diuron degradation reached 99.72% when the initial pH is acid (pH 4) whereas the diuron degradations with pH value of 7 (neutral) and 11 (base) are 98.72% and 93.23%, respectively. The rate of degradation increases, while the pH decreases as shown in Table 4.5. Therefore, the change of initial pH value affect to change of diuron degradation and the degradation of diuron is more effective under acidic condition [41].
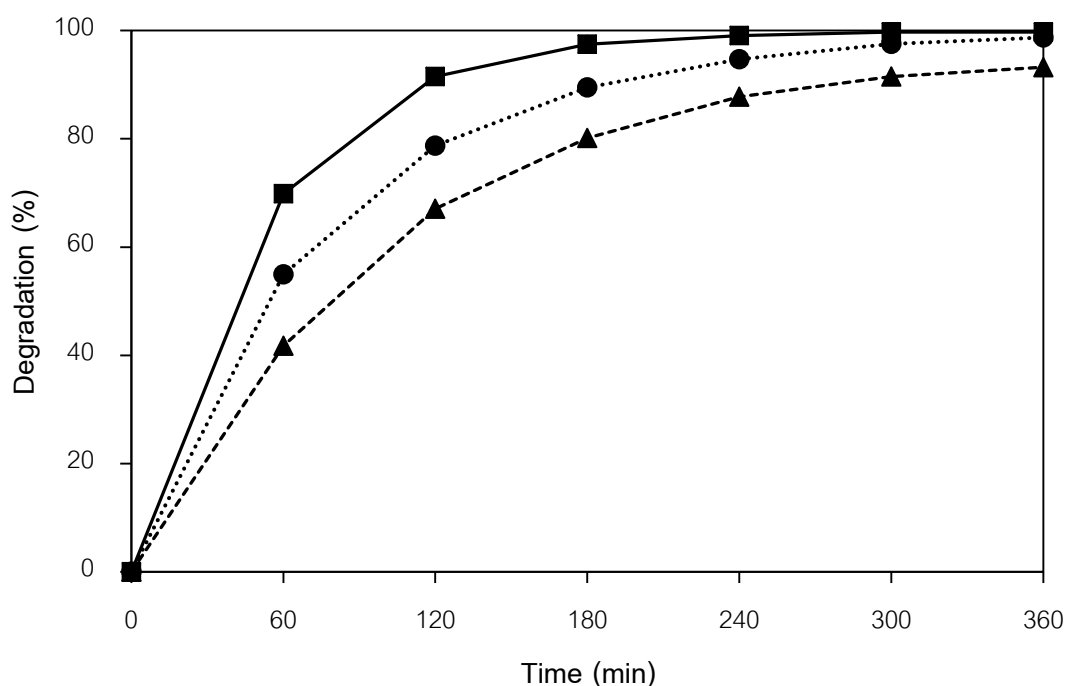
Figure 4.18 Influence of initial pH for the diuron degradation via EAOP: (■) pH 4, (●) pH 7, and, (▲) pH 11.

Table 4.5 Data the apparent rate constant (k_{app}) on the influence of pH value.

pH values	The apparent rate constant (min^{-1})	R^2
4	1.84×10^{-2}	0.997
7	1.25×10^{-2}	0.997
11	9.8×10^{-3}	0.998

The efficiency of diuron degradation increases, while the pH of solution decreases because more hydroxyl radicals are formed at low pH, as shown in form of hydrogen peroxide formation in Figure 4.19. The generation of hydroxyl radical via water oxidation is favored at pH lower than 9 [21]. In the basic solution, the hydroxyl radicals behave like a weak acid and interact with the hydroxide (OH^-) to form O^-, as followed in equation 4.18 [22]. Therefore, amount of hydroxyl radicals ($^\bullet OH$) decreases whereas the pH increases. In the acid solution, the disintegration of sulfuric acid (HSO_4^-) occurred then interacted with hydroxyl radical, as shown in equation 4.20. Therefore, amount of hydrogen peroxide slightly increased as resulting of hydroxyl radicals interacting with other ions.

$$^\bullet OH + OH^- \leftrightarrow O^- + H_2O^\bullet \qquad\qquad 4.19$$

$$HSO_4^- + {}^\bullet OH \leftrightarrow S_2O_8^{2-} + 2H_2O \qquad\qquad 4.20$$

Figure 4.20 shows that the efficiency of total organic carbon (TOC) removal is about 48% at acidic solution (pH 4). However, the TOC removal efficiencies at neutral solution (pH 7) and basic solution (pH 11) are 35% and 17%, respectively. Although diuron concentration decreases with time for result of HPLC, this reaction cannot complete all of the intermediate products.
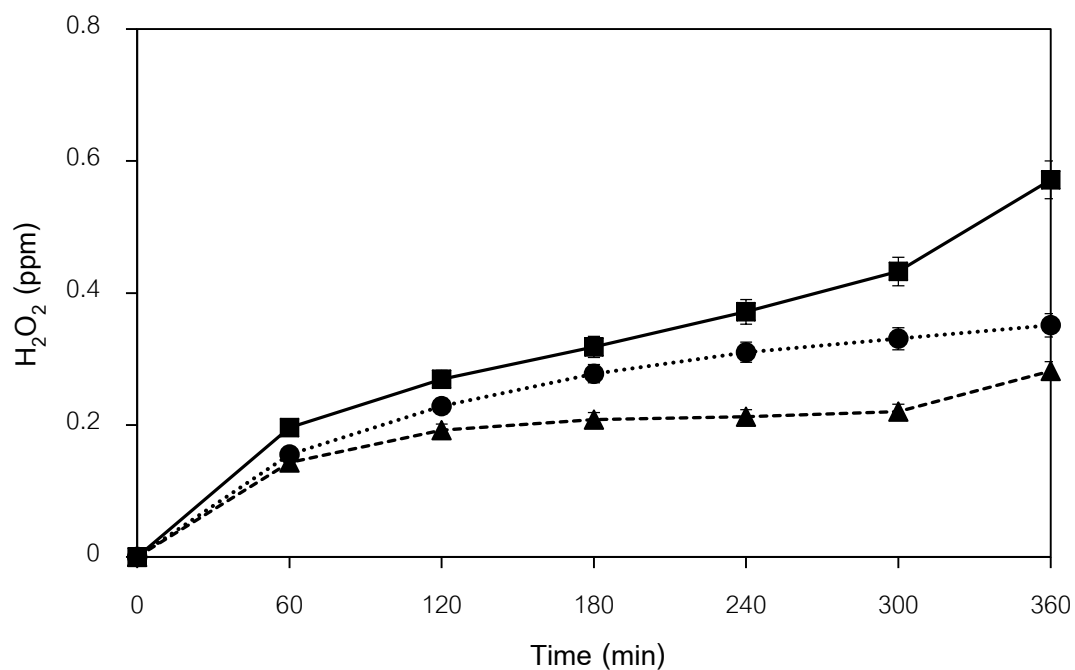
Figure 4.19 Hydrogen peroxide concentration in diuron on the influence of initial pH for the diuron degradation via EAOP: (■) pH 4, (●) pH 7, and, (▲) pH 11.
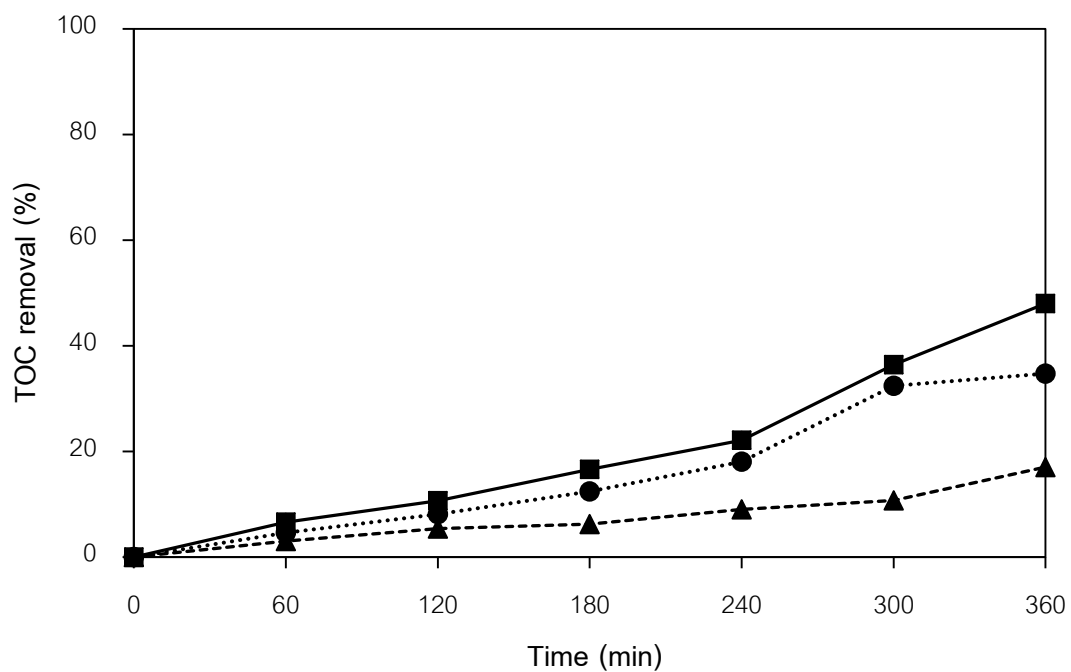
Figure 4.20 Total organic carbon on the influence of initial pH for the diuron degradation via EAOP: (■) pH 4, (●) pH 7, and, (▲) pH 11.

The intermediate products were detected using HPLC. Results in Figure 4.21 and 4.22 show peak intensity with time. At acidic solution (pH 4), seven compounds were detected as shown in Figure 4.21. The intermediate products were found at the retention time (R_T) of 1.45, 1.58, 1.74, 1.99, 2.19, 2.29, and 2.53 minutes, respectively.
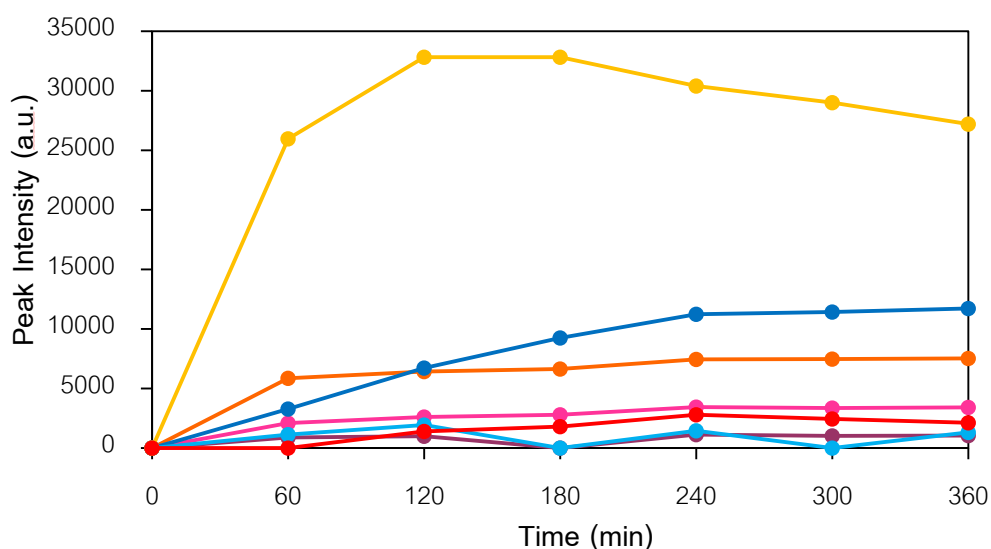
Figure 4.21 HPLC intermediate profile of diuron degradation via EAOP at acid solution (pH 4): (●) R_T = 1.45 min, (●) R_T = 1.58 min, (●) R_T = 1.74 min, (●) R_T = 1.99 min, (●) R_T = 2.19 min, (●) R_T = 2.29 min, and (●) R_T = 2.53 min.

Figure 4.22 shows intermediate profile with time at basic solution (pH 11). The intermediate products were found when at retention time (R_T) of 1.46, 1.57, 1.76, 2.00, 2.29, 2.57, and 2.87 minutes, respectively. For neutral solution (pH 7 as shown in Figure 4.9, the intermediate products were found at the retention time (R_T) of 1.48, 1.75, 1.90, 1.99, 2.29, 2.61, and 2.88 minutes, respectively. In addition to changing of pH value affects the efficiency of diuron removal, it also affects the intermediate product formation. Therefore, the degradation pathways should be different as pH is changed.

Figure 4.22 HPLC intermediate profile of diuron degradation via EAOP at base solution (pH 11): ($\bullet$) R_T = 1.46 min, ($\bullet$) R_T = 1.57 min, ($\bullet$) R_T = 1.76 min, ($\bullet$) R_T = 2.00 min, ($\bullet$) R_T = 2.29 min, ($\bullet$) R_T = 2.57 min, and ($\bullet$) R_T = 2.87 min.

4.6 The influence of electrode type.

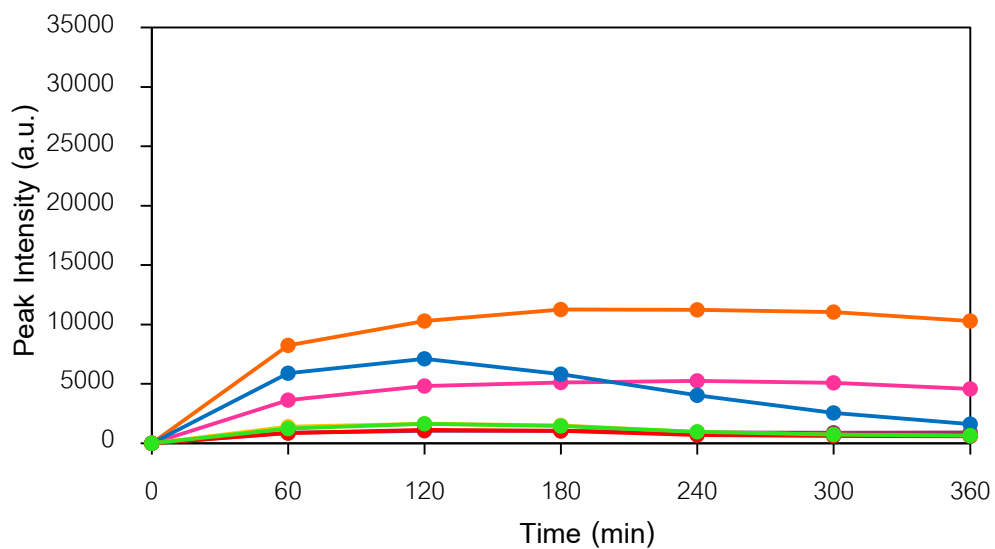The influence of electrode type is investigated by comparing between non-active anode as graphite and active anode as stainless steel at 50 mA of applied electric current, titanium plate as the cathode, 0.05 mol·L^{-1} of sodium sulfate (Na_2SO_4), and neutral initial solution (pH 7). Figure 4.23 shows that the percentage of diuron degradation is 98.72, 62.76, and 70.92 when the anode is graphite, stainless steel, and gold plated stainless steel, respectively. 'when comparison the diuron degradation between stainless steel and gold plate stainless steel, found that using an active anode has lower efficiency than using non-active anode and formed metal oxides due to changing oxidation state on surface anode. The metal oxides were generated from transition of oxygen (O_2) from hydroxyl radical ($^•OH$) to surface electrode (M) as shown in equation 4.21. The surface redox couple MO/M acted as a mediator in selective oxidation of diuron on the active anode as shown in equation 4.22 [12, 16].

$$M[^•OH] \rightarrow MO + H^+ + e^- \qquad\qquad 4.21$$

$$MO + R \rightarrow M + RO \qquad\qquad 4.22$$

Comparing the diuron degradation between graphite and gold plated stainless steel that the efficiency of diuron degradation was obviously different as result from different surface area, although they were both non-active anode. Graphite has higher surface area than gold plated stainless steel. If the anode has more surface area, more hydroxyl radicals can adsorb on the surface as much [48], hence, the diuron can be more degraded. This implied that more effective degradation resulted from using anode which had high surface area [49]. Therefore, the surface area was one of important influence on diuron degradation.

Figure 4.23 Influence of electrode type for the diuron degradation via EAOP: (●) graphite, (■) stainless steel, and, (▲) gold plated stainless steel.

Although graphite and gold plated stainless steel are both non-active anod, the apparent rate constant of graphite anode is 3.4 times that of the gold plated stainless steel anode (see Table 4.5). On the other hand, the apparent rate constant of non-active anode is more than that of active anode. However, the rate constant of gold plated stainless steel is slightly higher than that of stainless steel.

Table 4.6 Data of apparent rate constant (k_{app}) on influence of the electrode type.

Type of electrodes	The apparent rate constant (min^{-1})	R^2
Inactive anode		
Graphite	1.25×10^{-2}	0.997
Gold plated stainless steel	3.6×10^{-3}	0.970
Active anode		
Stainless steel	2.8×10^{-3}	0.992

Figure 4.24 shows the remained hydrogen peroxide (H_2O_2) after degradation resulted from different anodes. At active anode, the results showed that the hydrogen peroxide concentration increased throughout the first 4 hours. After that H_2O_2 concentration decreased as a result to occur side reaction. As results showed that concentration of hydrogen peroxide in diuron turned around efficiency of diuron degradation. This implied that more hydroxyl radicals destroyed diuron as a result hydrogen peroxide formation decreased.

Results of Figure 4.25 show that the efficiency of TOC removal is about 27% and 35% at graphite anode and stainless steel anode, respectively, indicating that the complete mineralization does not occur [16].

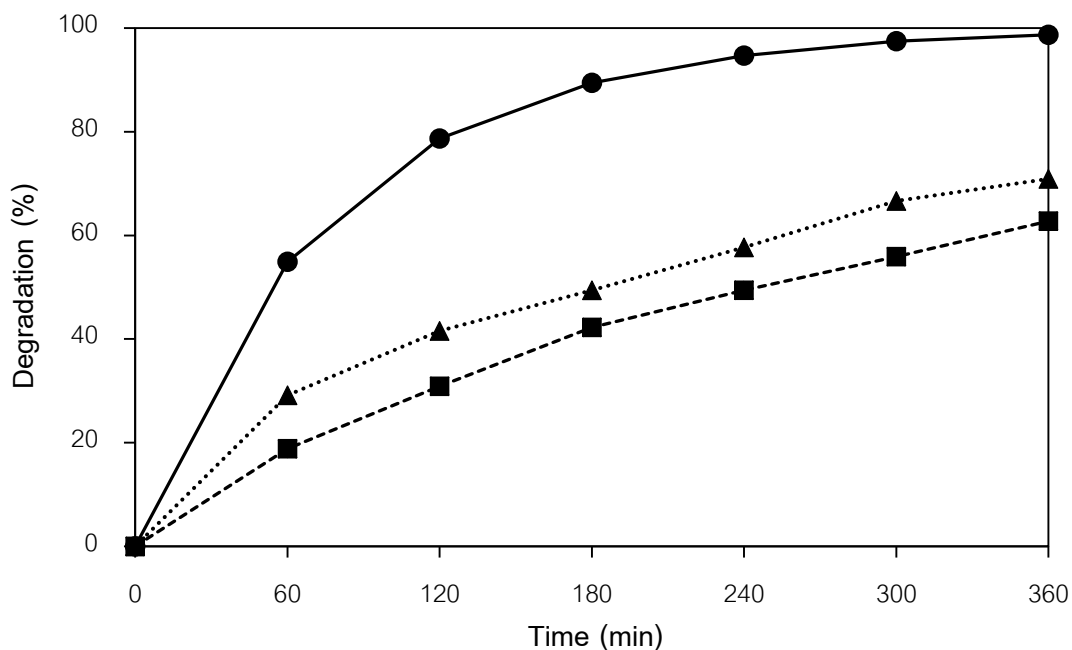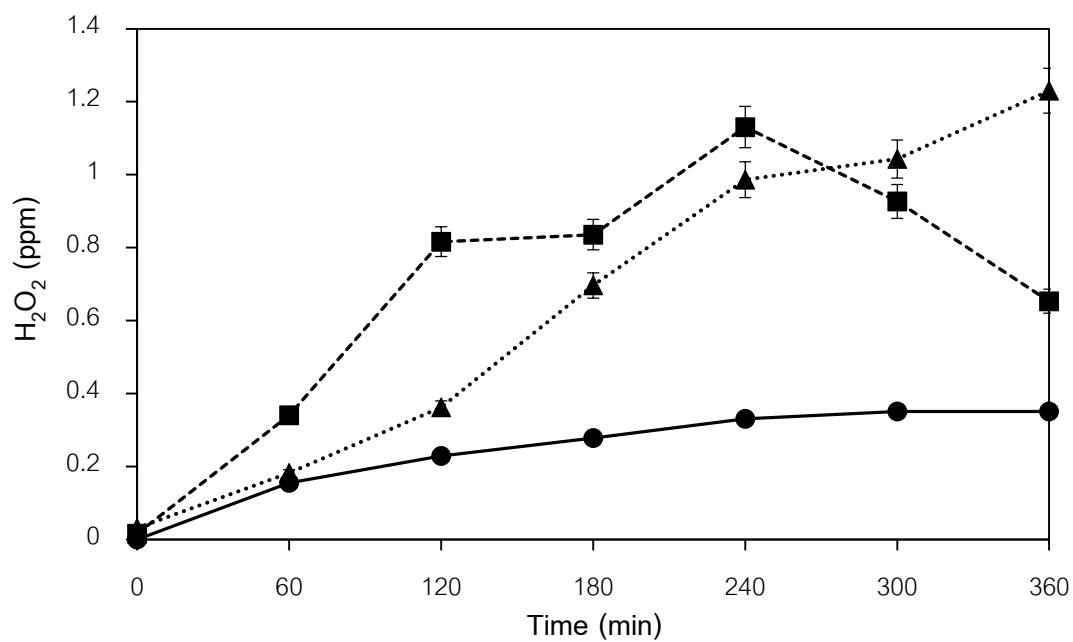**Figure 4.24** Hydrogen peroxide concentration in diuron on the influence of electrode type for the diuron degradation via EAOP: (●) graphite, (■) stainless steel, and, (▲) gold plated stainless steel.
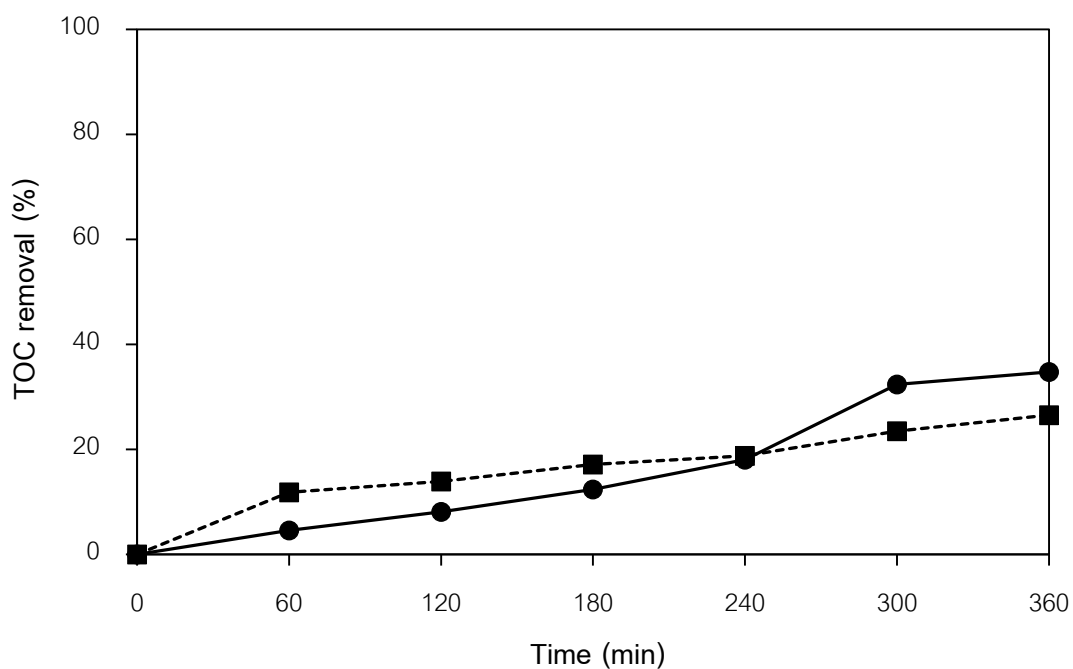
Figure 4.25 Total organic carbon on the influence of electrode type for the diuron degradation via EAOP: (●) graphite, (■) stainless steel.

The intermediate products were detected from HPLC. As results in Figure 4.26-4.27 show peak intensity with time. For gold plated stainless steel anode, four compounds were detected as shown in Figure 4.26. The intermediate products were found at the retention time (R_T) of 1.45, 1.99, 2.29, and 2.59 minutes, respectively.
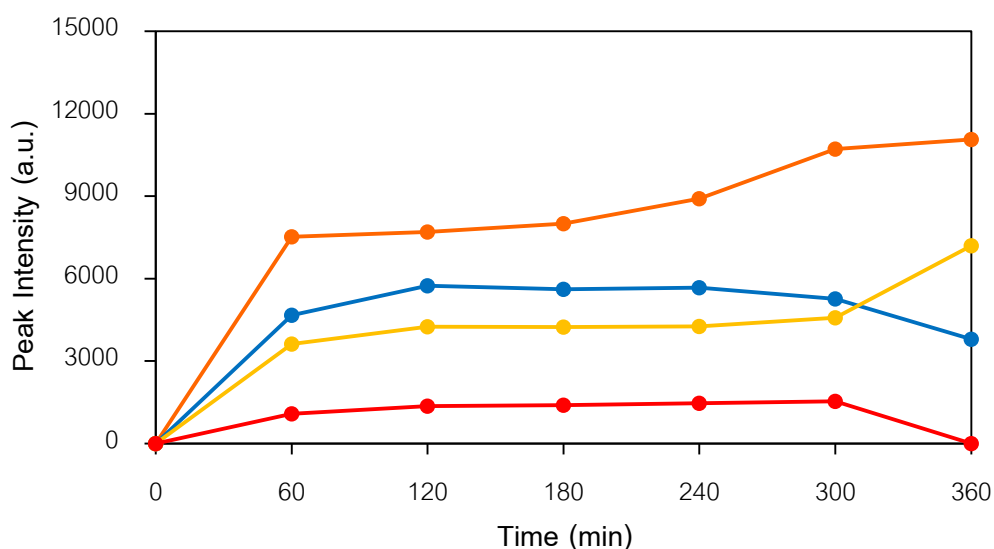
Figure 4.26 HPLC intermediate profile of diuron degradation via EAOP by using inactive anode (gold plated stainless steel): (●) R_T = 1.45 min, (●) R_T = 1.99 min, (●) R_T = 2.29 min, and (●) R_T = 2.59 min.

Figure 4.27 shows intermediate profile with time when anode is stainless steel. The intermediate products were found when at retention time (R_T) of 1.57, 2.00, 2.30, 2.83, 3.76, 4.52, 5.23, 5.56 and 5.74 minutes, respectively. For graphite anode as shown in Figure 4.9, the intermediate products were found at the retention time (R_T) of 1.48, 1.75, 1.90, 1.99, 2.29, 2.61, and 2.88 minutes, respectively. Results showed that Intermediate products were formed obviously different. Therefore, the different electrode affected to intermediate product formation.

Figure 4.27 HPLC intermediate profile of diuron degradation via EAOP by using active anode (stainless steel): (●) R_T = 1.57 min, (●) R_T =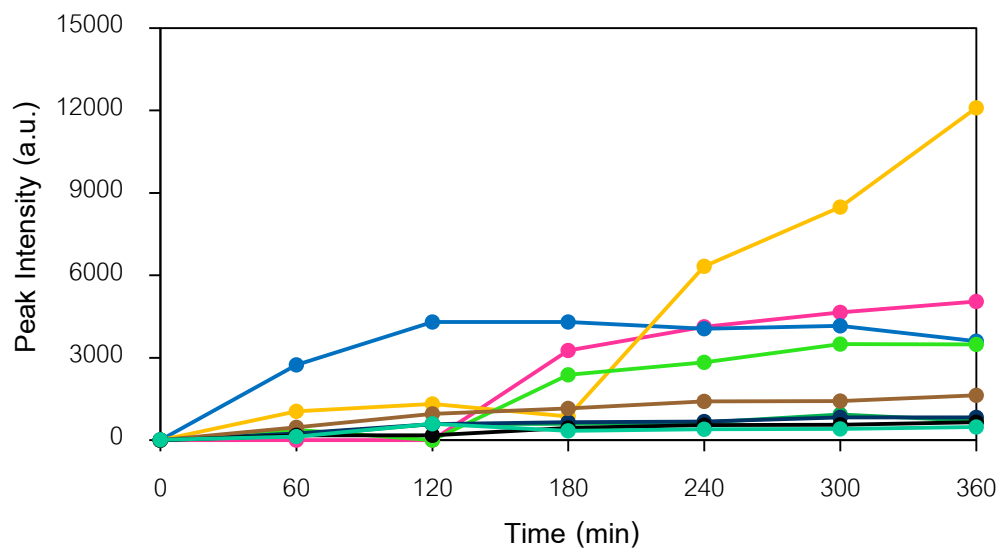 2.00 min, (●) R_T = 2.30 min, (●) R_T = 2.83 min, (●) R_T = 3.76 min, (●) R_T = 4.52 min, (●) R_T = 5.23 min, (●) R_T = 5.56 min, and (●) R_T = 5.74 min.

4.7 The influence of temperature.

To investigate the influence of temperature on diuron degradation, this experiment varied temperatures at 10 °C, 30 °C, and 60 °C, respectively. All of conditions were controlled at 50 mA of applied electric current and 0.05 mol·L^{-1}. At 360 minutes, the percentage of diuron degradation is 88.37, 98.72, and 99.75 when the temperature is 10 °C, 30 °C, and 60 °C, respectively. Increasing temperature was mainly cause for increasing of diuron degradation (shown in Figure 4.28) and kinetic constant [50, 51], so rate of reaction also increased. Table 4.7 shows the apparent rate constants at the different temperatures, indicating that the kinetic rate depends on temperature following Arrhenius's law [41] which is shown in equation 4.23. The activation energy of this reaction is 17.73 kJ·mol^{-1} and calculation is shown in Appendix C. Comparing this system to hydrolysis, found that this system requires lower the activation energy, so this is indicated that EAOP can easily occur.

$$k = k_0 e^{\frac{-E}{RT}} \qquad\qquad 4.23$$

Table 4.7 Data of the apparent rate constant (k_{app}) on the influence of temperature.

Temperature (°C)	The apparent rate constant (min^{-1})	R^2
10	6.0×10^{-3}	0.967
30	1.25×10^{-2}	0.997
60	1.89×10^{-2}	0.998

Figure 4.28 Influence of temperature for the diuron degradation via EAOP: (▲) 10 °C, (●) 30 °C, and, (■) 60 °C.

Figure 4.29 and 4.30 showed that concentration of hydrogen peroxide in diuron was lower than concentration of hydrogen peroxide in DI water a hydroxyl radicals reacted with diuron. Increasing hydrogen peroxide formation is resulting from rising temperature. At high temperature, the persulfate ions ($S_2O_8^{2-}$), which were formed from oxidation of sulfate ions (SO_4^{2-}), were hydrolyzed to SO_4^{2-} and H_2O_2, as shown in equation 4.24-4.26 Therefore, increasing temperature also increases the amount of hydrogen peroxide [15, 42].

$$2SO_4^{2-} \leftrightarrow S_2O_8^{2-} + 2e^- \qquad\qquad 4.24$$

$$S_2O_8^{2-} + H_2O \rightarrow SO_5^{2-} + SO_4^{2-} + 2H^+ \qquad\qquad 4.25$$

$$SO_5^{2-} + H_2O \rightarrow H_2O_2 + SO_4^{2-} \qquad\qquad 4.26$$

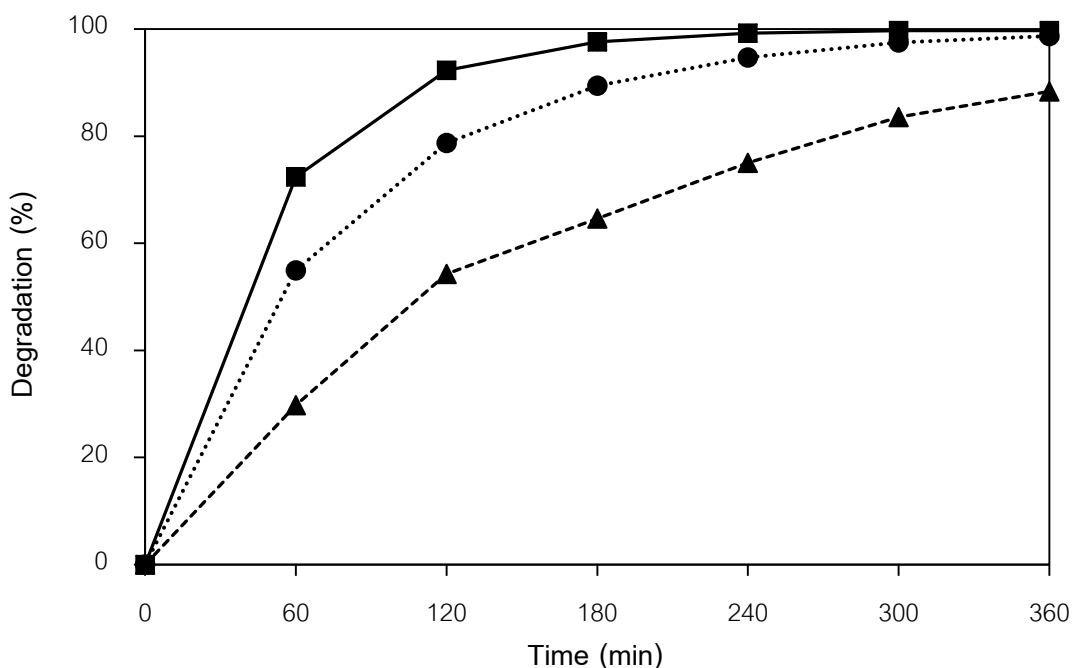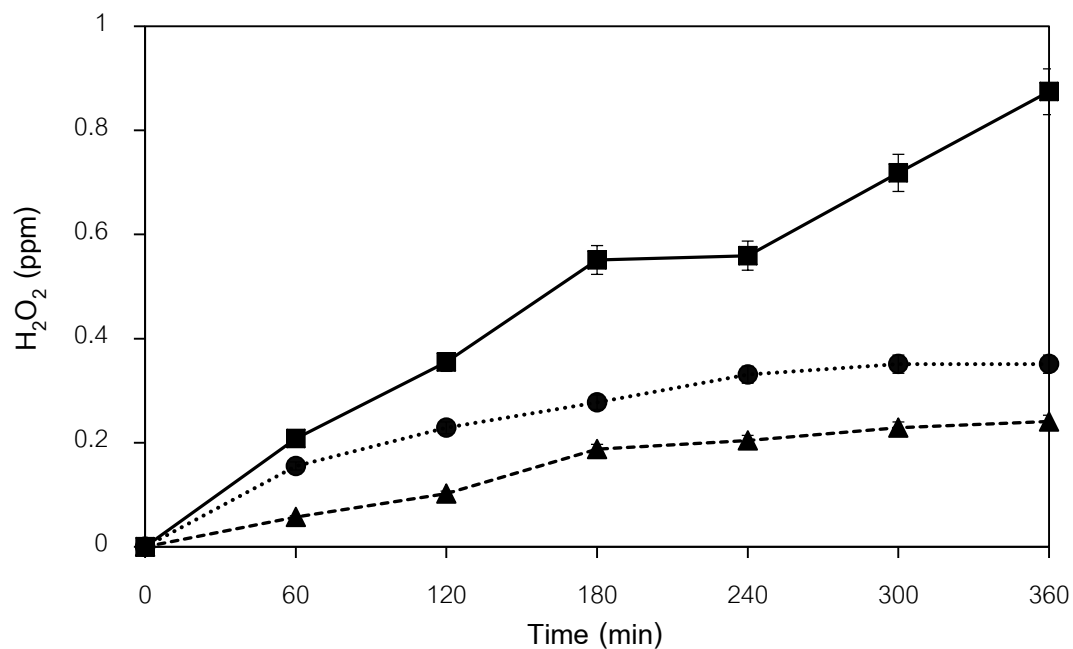**Figure 4.29** Hydrogen peroxide concentration in diuron on the influence of temperature for the diuron degradation via EAOP: (▲) 10 °C, (●) 30 °C, and, (■) 60 °C.
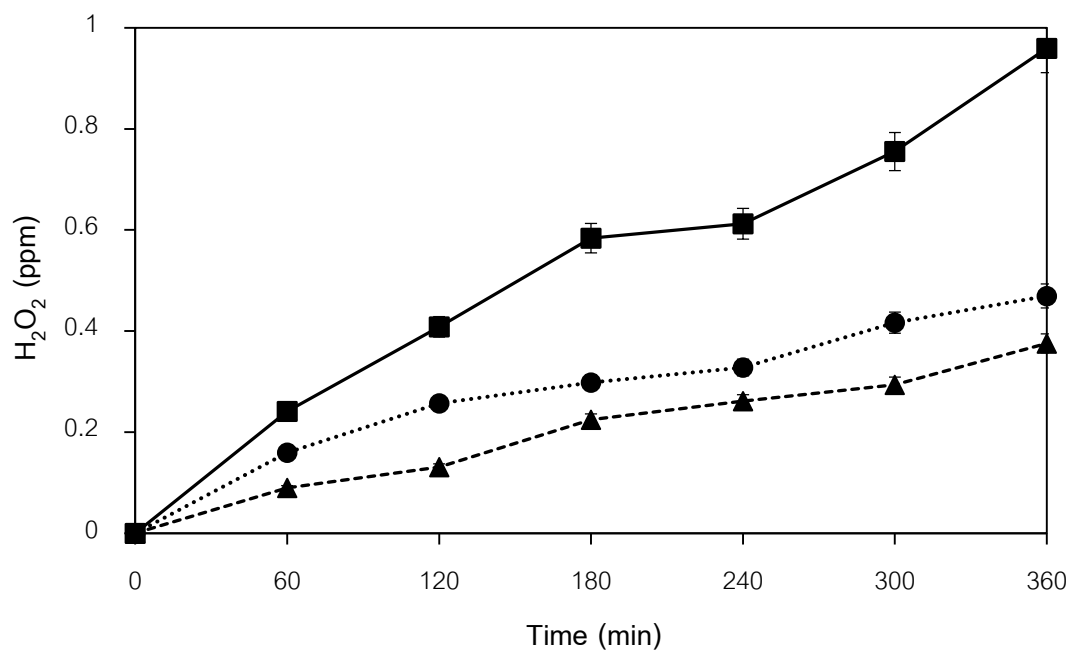
Figure 4.30 Hydrogen peroxide concentration in DI water on the influence of temperature: (▲) 10 °C, (●) 30 °C, and, (■) 60 °C.

Figure 4.31 shows the efficiency of total organic carbon (TOC) removal is about 30 %, 35%, and 48% when temperature is 10 °C, 30 °C, and 60 °C, respectively. Although diuron concentration decreases with time from the result of HPLC, this reaction cannot completely degraded all of intermediate products.
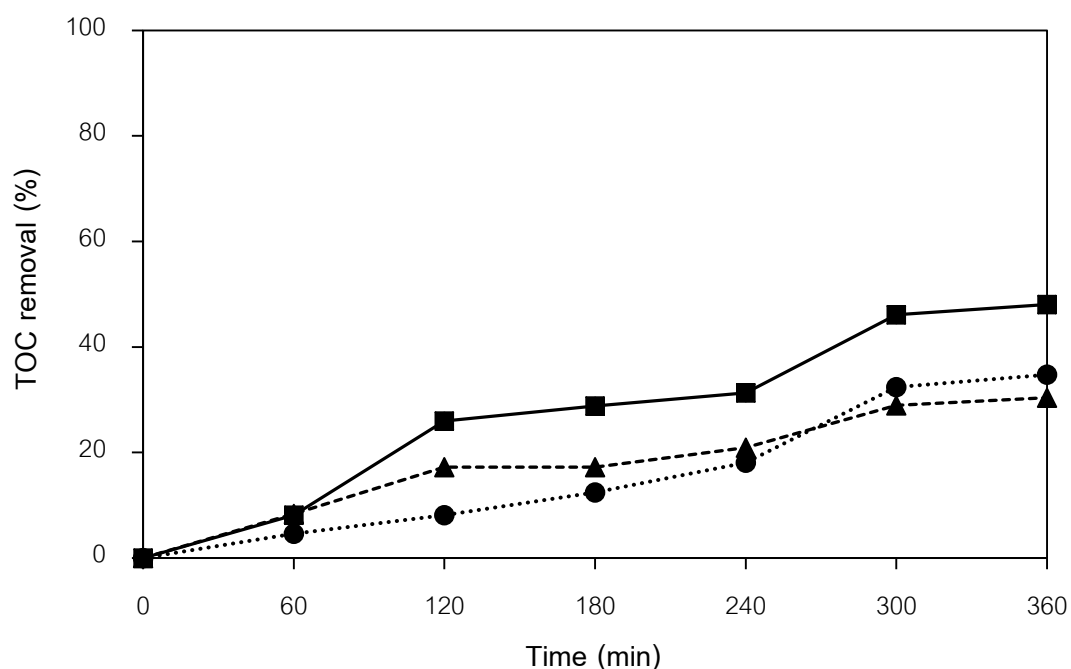
Figure 4.31 Total organic carbon on the influence of anode type for the diuron degradation via EAOP: (▲) 10 °C, (●) 30 °C, and, (■) 60 °C.

The intermediate products were detected from HPLC. Results in Figure 4.32 and 4.33 show peak intensity with time. At 10 °C, six compounds were detected as shown in Figure 4.32. The intermediate products were found at the retention time (R_T) of 1.50, 1.59, 2.08, 2.30, 2.63, and 2.97 minutes, respectively.

Figure 4.33 shows intermediate profile with time when temperature is 60 °C. The intermediate products were found when at retention time (R_T) of 1.49, 1.59, 2.00, 2.30,

2.63, and 2.96 minutes, respectively. At 30 °C as shown in Figure 4.9, the intermediate products were found at the retention time (R_T) of 1.48, 1.75, 1.90, 1.99, 2.29, 2.61, and 2.88 minutes, respectively. Therefore, influence of temperature is slightly important for intermediate products of diuron degradation and the degradation pathway should difference with temperature.

Figure 4.32 HPLC intermediate profile of diuron degradation via EAOP at 10 °C: ($\bullet$) R_T = 1.50 min, ($\bullet$) R_T = 1.59 min, ($\bullet$) R_T = 2.08 min, ($\bullet$) R_T = 2.30 min, ($\bullet$) R_T = 2.63 min and ($\bullet$) R_T = 2.97 min.

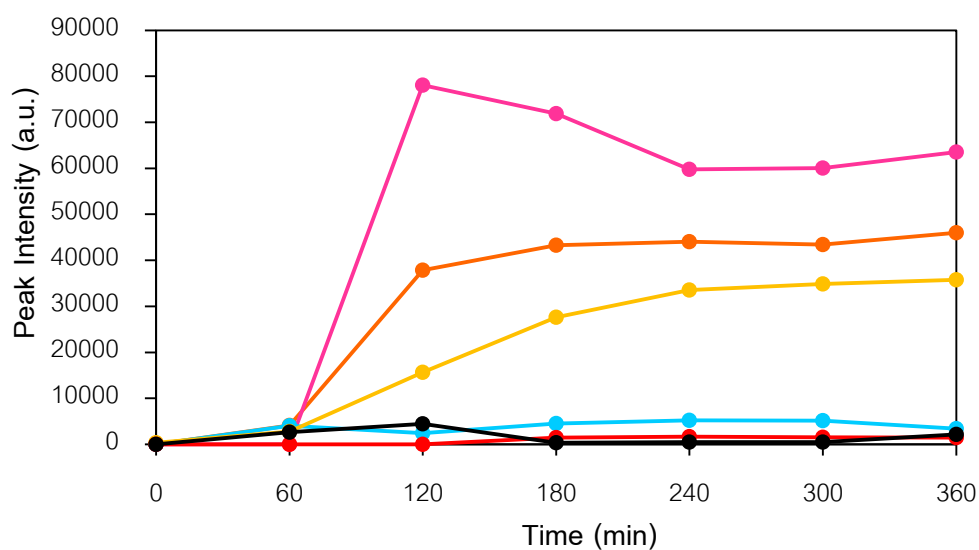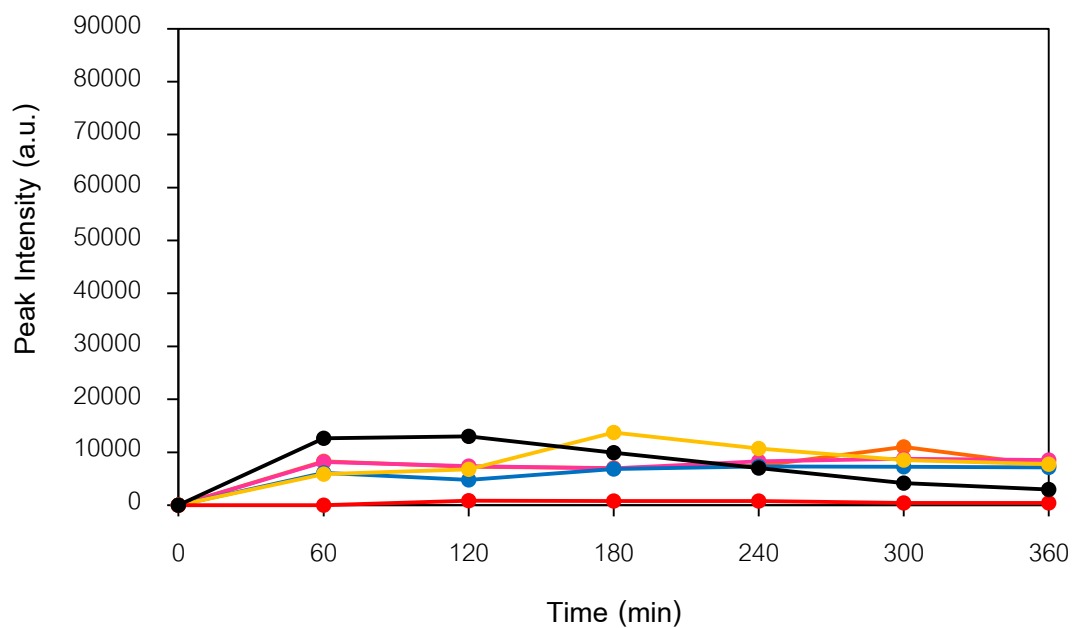**Figure 4.33** HPLC intermediate profile of diuron degradation via EAOP at 60 °C: (●) R_T = 1.49 min, (●) R_T = 1.59 min, (●) R_T = 2.00 min, (●) R_T = 2.30 min, (●) R_T = 2.63 min and (●) R_T = 2.96 min.

CHAPTER V

CONCLUSION AND RECOMMENDATIONS

This chapter has 3 mainly section involving summary of the results, conclusion, and recommendation for future work.

5.1 Summary of the results

1. The diuron can be degraded via electrochemical advanced oxidation process (EAOP).

2. The diuron structure was destroyed by hydroxyl radicals ($^{\bullet}$OH), which generated from water oxidation.

3. While diuron degradation took place, hydrogen peroxides (H_2O_2) formed by recombination of hydroxyl radicals.

4. These parameters such as initial pH, temperature, applied electric current, type of electrolyte, and type of electrode have affected to hydroxyl radical formation.

5. In this work, the reaction follows the pseudo-first-order kinetic.

6. The mass transfer resistance in the system was negligible when the mixing speed was more than 1,200 rpm.

7. The influence of anion, type of electrode, and temperature affect to production of intermediate products.

5.2 Conclusion

Diuron can be degraded via electrochemical advanced oxidation process (EAOP) as a result from hydroxyl radicals which were generated from water oxidation at anode surface. The hydroxyl radicals attack diuron structure, so the degradation took place. The hydrogen peroxides which were resulted from recombination of hydroxyl radicals were detected in the solution and were used to confirm formation of hydroxyl radical. The efficiency of diuron removal depends on the influence of initial pH, applied electric current, type of electrode, temperature, and type of electrolyte. The reaction generally follows the pseudo-first-order kinetic.

5.3 Recommendations for the future work

1. Identification of intermediate products of diuron degradation by using liquid chromatography-tandem mass spectrometry (LC-MS/MS).

2. Measuring the amount of anions from electrolyte.

3. Investigation of toxicity of product.

REFERENCES

[1]   B.P. Chaplin, Critical review of electrochemical advanced oxidation processes for water treatment applications, Environ Sci Process Impacts. 16 (2014) 1182-203.

[2]   I. Sires, E. Brillas, M.A. Oturan, M.A. Rodrigo, and M. Panizza, Electrochemical advanced oxidation processes: today and tomorrow. A review, Environ Sci Pollut Res Int. 21 (2014) 8336-67.

[3]   J.S. Wessels and R. Van Der Veen, The action of some derivatives of phenylurethan and of 3-phenyl-1, 1-dimethylurea on the Hill reaction, Biochimica et biophysica acta. 19 (1956) 548-549.

[4]   D.A. Laskowski, R.L. Swann, P.J. McCall, and H.D. Bidlack, *Soil degradation studies*, in *Residue Reviews*, F. Gunther and J. Gunther, Editors. 1983, Springer New York. p. 139-147.

[5]   J.A. Field, R.L. Reed, T.E. Sawyer, S.M. Griffith, and P.J. Wigington, Diuron Occurrence and Distribution in Soil and Surface and Ground Water Associated with Grass Seed Production, Journal of Environmental Quality. 32 (2003) 171-179.

[6]   H. Okamura, I. Aoyama, Y. Ono, and T. Nishida, Antifouling herbicides in the coastal waters of western Japan, Marine Pollution Bulletin. 47 (2003) 59-67.

[7]   K. Jüttner, U. Galla, and H. Schmieder, Electrochemical approaches to environmental problems in the process industry, Electrochimica Acta. 45 (2000) 2575-2594.

[8]   J. Feng, D.C. Johnson, S.N. Lowery, and J.J. Carey, Electrocatalysis of Anodic Oxygen‑Transfer Reactions Evolution of Ozone, Journal of The Electrochemical Society. 141 (1994) 2708-2711.

[9]   J. Feng and D.C. Johnson, Electrocatalysis of Anodic Oxygen‑Transfer Reactions Fe‑Doped Beta‑Lead Dioxide Electrodeposited on Noble Metals, Journal of The Electrochemical Society. 137 (1990) 507-510.

[10]   H. Chang and D.C. Johnson, Electrocatalysis of Anodic Oxygen-Transfer Reactions Ultrathin Films of Lead Oxide on Solid Electrodes, Journal of The Electrochemical Society. 137 (1990).

[11]   H. Chang and D.C. Johnson, Electrocatalysis of Anodic Oxygen-Transfer Reactions Activation of Formula Electrodes in Formula by Addition of Bismuth(III) and Arsenic(III,V), Journal of The Electrochemical Society. 137 (1990) 2452-2457.

[12]   C.A. Martinez-Huitle and S. Ferro, Electrochemical oxidation of organic pollutants for the wastewater treatment: direct and indirect processes, Chem Soc Rev. 35 (2006) 1324-40.

[13]   E. Brillas, I. Sires, and M.A. Oturan, Electro-Fenton process and related electrochemical technologies based on Fenton's reaction chemistry, Chem Rev. 109 (2009) 6570-631.

[14]   W. Khongthon, G. Jovanovic, A. Yokochi, P. Sangvanich, and V. Pavarajarn, Degradation of diuron via an electrochemical advanced oxidation process in a microscale-based reactor, Chemical Engineering Journal. 292 (2016) 298-307.

[15]   C. Barrera-Díaz, P. Cañizares, F.J. Fernández, R. Natividad, and M.A. Rodrigo, Electrochemical advanced oxidation processes: An overview of the current applications to actual industrial effluents, Journal of the Mexican Chemical Society. 58 (2014) 256-275.

[16]   M. Panizza and G. Cerisola, Direct And Mediated Anodic Oxidation of Organic Pollutants, Chemical Reviews. 109 (2009) 6541-6569.

[17]   N. Borràs, R. Oliver, C. Arias, and E. Brillas, Degradation of Atrazine by Electrochemical Advanced Oxidation Processes Using a Boron-Doped Diamond Anode, The Journal of Physical Chemistry A. 114 (2010) 6613-6621.

[18]   C. Comninellis, Electrocatalysis in the electrochemical conversion/combustion of organic pollutants for waste water treatment, Electrochimica Acta. 39 (1994) 1857-1862.

[19]   F.L. Guzmán-Duque, R.E. Palma-Goyes, I. González, G. Peñuela, and R.A. Torres-Palma, Relationship between anode material, supporting electrolyte and current

density during electrochemical degradation of organic compounds in water, Journal of Hazardous Materials. 278 (2014) 221-226.

[20]   C. Tan, N. Gao, W. Chu, C. Li, and M.R. Templeton, Degradation of diuron by persulfate activated with ferrous ion, Separation and Purification Technology. 95 (2012) 44-48.

[21]   T.A. Enache, A.-M. Chiorcea-Paquim, O. Fatibello-Filho, and A.M. Oliveira-Brett, Hydroxyl radicals electrochemically generated in situ on a boron-doped diamond electrode, Electrochemistry Communications. 11 (2009) 1342-1345.

[22]   L.M. Dorfman, U.S.N.B.o. Standards, and G.E. Adams, *Reactivity of the Hydroxyl Radical in Aqueous Solutions*. 1973: U.S. Department of Commerce, National Bureau of Standards.

[23]   Y. Samet, L. Agengui, and R. Abdelhédi, Electrochemical degradation of chlorpyrifos pesticide in aqueous solutions by anodic oxidation at boron-doped diamond electrodes, Chemical Engineering Journal. 161 (2010) 167-172.

[24]   A.L. Giraldo, E.D. Erazo-Erazo, O.A. Flórez-Acosta, E.A. Serna-Galvis, and R.A. Torres-Palma, Degradation of the antibiotic oxacillin in water by anodic oxidation with Ti/IrO2 anodes: Evaluation of degradation routes, organic by-products and effects of water matrix components, Chemical Engineering Journal. 279 (2015) 103-114.

[25]   S. Giacomazzi and N. Cochet, Environmental impact of diuron transformation: a review, Chemosphere. 56 (2004) 1021-32.

[26]   S. Salvestrini, P. Di Cerbo, and S. Capasso, Kinetics of the chemical degradation of diuron, Chemosphere. 48 (2002) 69-73.

[27]   S. Hussain, M. Arshad, D. Springael, S.R. SøRensen, G.D. Bending, M. Devers-Lamrani, Z. Maqbool, and F. Martin-Laurent, Abiotic and Biotic Processes Governing the Fate of Phenylurea Herbicides in Soils: A Review, Critical Reviews in Environmental Science and Technology. 45 (2015) 1947-1998.

[28]   S.R. Sorensen, R.K. Juhler, and J. Aamand, Degradation and mineralisation of diuron by Sphingomonas sp. SRS2 and its potential for remediating at a realistic microg L(-1) diuron concentration, Pest Manag Sci. 69 (2013) 1239-44.

[29]   V. Travkin, B.P. Baskunov, E.L. Golovlev, M.G. Boersma, S. Boeren, J. Vervoort, W.J.H. van Berkel, I.M.C.M. Rietjens, and L.A. Golovleva, Reductive deamination as a new step in the anaerobic microbial degradation of halogenated anilines, FEMS Microbiology Letters. 209 (2002) 307--312.

[30]   V.V.M. Travkin, I.I.P. Solyanikova, I.I.M.C.M. Rietjens, J.J. Vervoort, W.W.J.H. van Berkel, and L.L.A. Golovleva, Degradation of 3,4-Dichloro- and 3,4-Difluoroaniline by Pseudomonas fluorescens 26-K, Journal of Environmental Science and Health, Part B. 38 (2003) 121-132.

[31]   H. Katsumata, M. Sada, Y. Nakaoka, S. Kaneco, T. Suzuki, and K. Ohta, Photocatalytic degradation of diuron in aqueous solution by platinized TiO2, J Hazard Mater. 171 (2009) 1081-7.

[32]   D.S. Bhatkhande, V.G. Pangarkar, and A.A.C.M. Beenackers, Photocatalytic degradation for environmental applications – a review, Journal of Chemical Technology & Biotechnology. 77 (2002) 102--116.

[33]   G. Zhao, P. Li, F. Nong, M. Li, J. Gao, and D. Li, Construction and High Performance of a Novel Modified Boron-Doped Diamond Film Electrode Endowed with Superior Electrocatalysis, The Journal of Physical Chemistry C. 114 (2010) 5906-5913.

[34]   M.A. Oturan, M.C. Edelahi, N. Oturan, K. El kacemi, and J.-J. Aaron, Kinetics of oxidative degradation/mineralization pathways of the phenylurea herbicides diuron, monuron and fenuron in water during application of the electro-Fenton process, Applied Catalysis B: Environmental. 97 (2010) 82-89.

[35]   M.A. Oturan, N. Oturan, M.C. Edelahi, F.I. Podvorica, and K.E. Kacemi, Oxidative degradation of herbicide diuron in aqueous medium by Fenton's reaction based advanced oxidation processes, Chemical Engineering Journal. 171 (2011) 127-135.

[36] T. Wu and J.D. Englehardt, A New Method for Removal of Hydrogen Peroxide Interference in the Analysis of Chemical Oxygen Demand, Environmental Science & Technology. 46 (2012) 2291-2298.

[37] A. Fabiańska, A. Ofiarska, A. Fiszka-Borzyszkowska, P. Stepnowski, and E.M. Siedlecka, Electrodegradation of ifosfamide and cyclophosphamide at BDD electrode: Decomposition pathway and its kinetics, Chemical Engineering Journal. 276 (2015) 274-282.

[38] E.J. Ruiz, C. Arias, E. Brillas, A. Hernández-Ramírez, and J.M. Peralta-Hernández, Mineralization of Acid Yellow 36 azo dye by electro-Fenton and solar photoelectro-Fenton processes with a boron-doped diamond anode, Chemosphere. 82 (2011) 495-501.

[39] R. Salazar, S. Garcia-Segura, M.S. Ureta-Zañartu, and E. Brillas, Degradation of disperse azo dyes from waters by solar photoelectro-Fenton, Electrochimica Acta. 56 (2011) 6371-6379.

[40] A.R. Pipi, I. Sires, A.R. De Andrade, and E. Brillas, Application of electrochemical advanced oxidation processes to the mineralization of the herbicide diuron, Chemosphere. 109 (2014) 49-55.

[41] F.C. Moreira, R.A.R. Boaventura, E. Brillas, and V.J.P. Vilar, Electrochemical advanced oxidation processes: A review on their application to synthetic and real wastewaters, Applied Catalysis B: Environmental. 202 (2017) 217-261.

[42] H. Rubí-Juárez, S. Cotillas, C. Sáez, P. Cañizares, C. Barrera-Díaz, and M.A. Rodrigo, Removal of herbicide glyphosate by conductive-diamond electrochemical oxidation, Applied Catalysis B: Environmental. 188 (2016) 305-312.

[43] I. Katsounaros and G. Kyriacou, Influence of the concentration and the nature of the supporting electrolyte on the electrochemical reduction of nitrate on tin cathode, Electrochimica Acta. 52 (2007) 6412-6420.

[44]   M.S. Saha, T. Furuta, and Y. Nishiki, Conversion of carbon dioxide to peroxycarbonate at boron-doped diamond electrode, Electrochemistry Communications. 6 (2004) 201-204.

[45]   W. Khongthon and V. Pavarajarn, Effect of Nitrate and Sulfate Contamination on Degradation of Diuron via Electrochemical Advanced Oxidation in a Microreactor, Engineering Journal. 20 (2016) 25-34.

[46]   W. Khongthon, *DEGRADATION OF DIURON VIA AN ELECTROCHEMICAL ADVANCED OXIDATION PROCESS IN A MICROSCALE-BASED REACTOR*, in *Chemical Engineering*. 2016, Chulalongkorn University. p. 182.

[47]   H.B. Ammar, M.B. Brahim, R. Abdelhédi, and Y. Samet, Green electrochemical process for metronidazole degradation at BDD anode in aqueous solutions via direct and indirect oxidation, Separation and Purification Technology. 157 (2016) 9-16.

[48]   A.M. Polcaro and S. Palmas, Electrochemical Oxidation of Chlorophenols, Industrial & Engineering Chemistry Research. 36 (1997) 1791-1798.

[49]   F. Yi and S. Chen, Electrochemical treatment of alizarin red S dye wastewater using an activated carbon fiber as anode material, Journal of Porous Materials. 15 (2008) 565-569.

[50]   B. Boye, M.M. Dieng, and E. Brillas, Degradation of Herbicide 4-Chlorophenoxyacetic Acid by Advanced Electrochemical Oxidation Methods, Environmental Science & Technology. 36 (2002) 3030-3035.

[51]   S. Malato, P. Fernández-Ibáñez, M.I. Maldonado, J. Blanco, and W. Gernjak, Decontamination and disinfection of water by solar photocatalysis: Recent overview and trends, Catalysis Today. 147 (2009) 1-59.

APPENDICES

APPENDIX A

CALIBRATION DATA ANALYSIS

A.1 Calibration curve of the diuron.

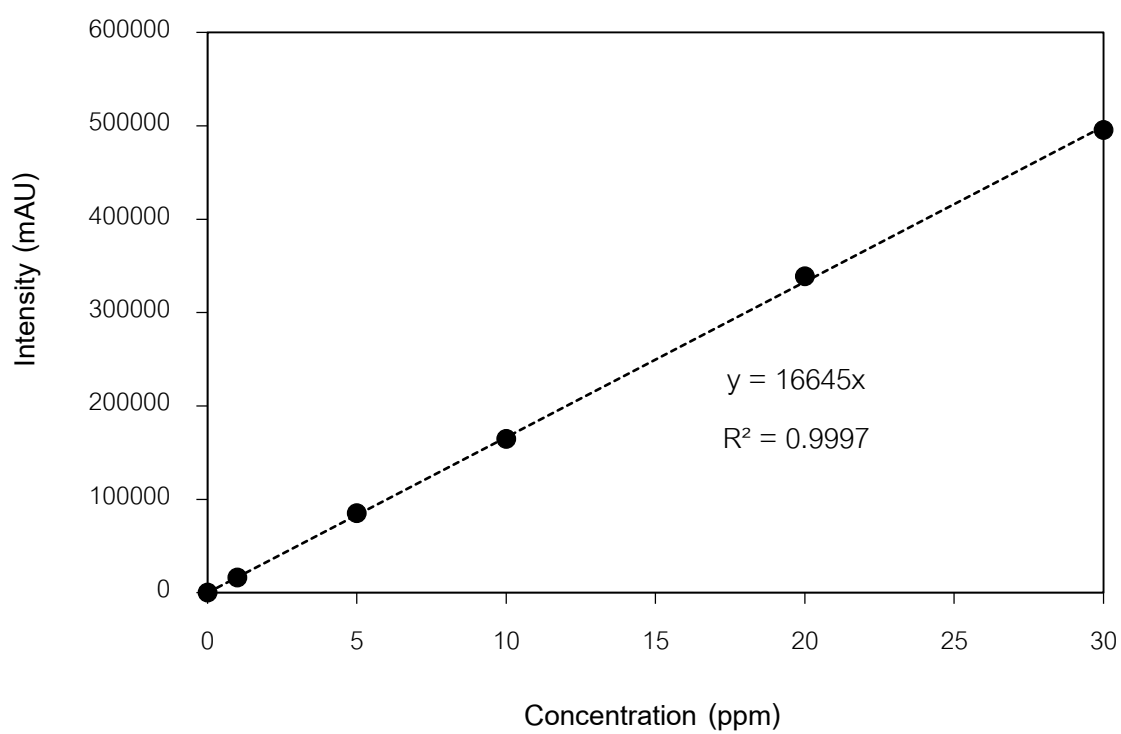
$y = 16645x$

$R^2 = 0.9997$

Figure A.1 Calibration curve of the diuron.

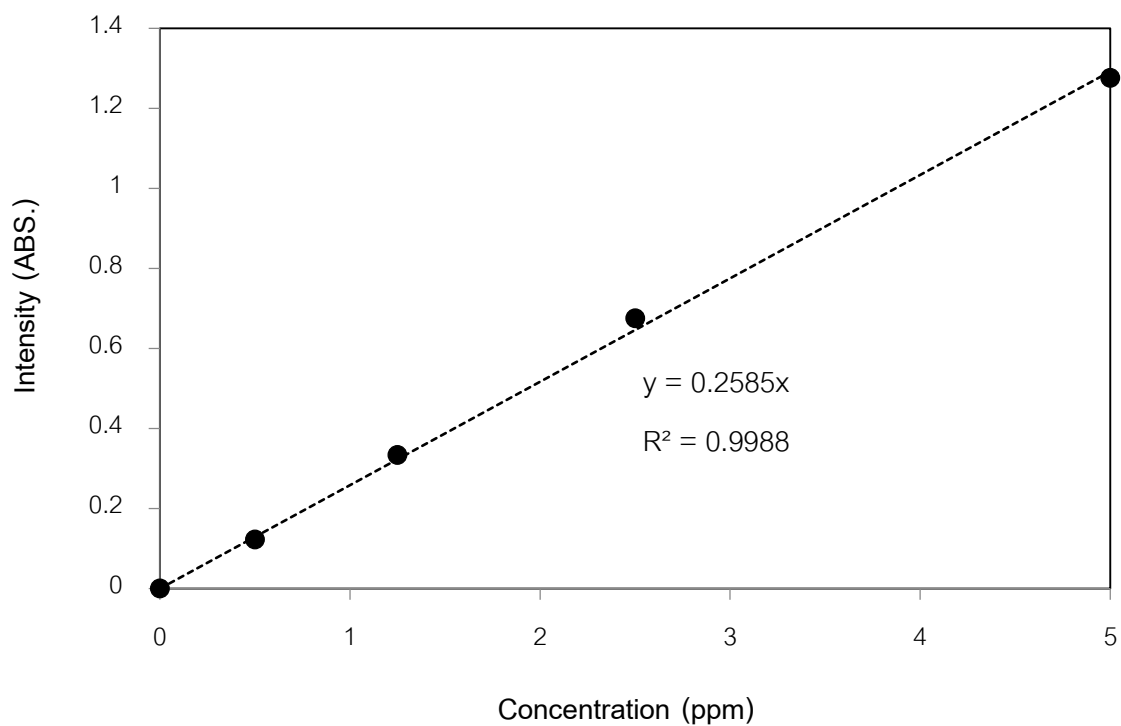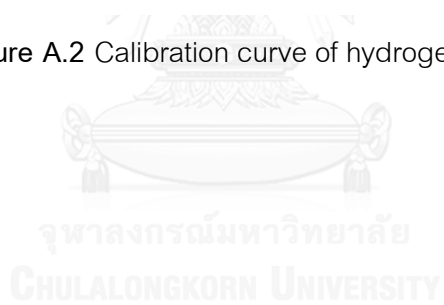A.2 Calibration curve of hydrogen peroxide.

Figure A.2 Calibration curve of hydrogen peroxide.

APPENDIX B

CHEMICAL PREPARATION

B.1 Determination of hydrogen peroxide (H_2O_2).

1. Preparation of A reagent.

- Added 0.01 g of ammonium molybdate, 0.1 g of sodium hydroxide, and 3.3 g of potassium chloride into the volumetric flask.

- Finally, added deionized water until the total volume is 50 ml.

2. Preparation of B reagent.

- Added 1 g of potassium hydrogen phthalate into the volumetric flask.

- Finally, added deionized water until the total volume is 50 ml.

3. Measured the hydrogen peroxide via ultraviolet-visible spectroscopy (UV-vis).

- Mixed 1 ml of the sample, 1 ml of A reagent, and 1 ml of B reagent.

- Used 3 ml of deionized water is blank.

- The H_2O_2 is detected in wavelength at 350 nanometers.

APPENDIX C

CALCULATION OF THE ACTIVATION ENERGY

The activation energy of the reaction (E) can calculated by Arrhenius's law, as followed in equation C.1.and C.2.

$$k = k_0 e^{\frac{-E}{RT}} \hspace{5cm} \text{C.1}$$

$$\ln k = \ln k_0 - \frac{E}{RT} \hspace{5cm} \text{C.2}$$

where: k   is the reaction rate coefficient.

k_0 is the frequency factor for the reaction.

E   is the activation energy of the reaction.

R   is the universal gas constant (8.314 J·mol-1·K-1).

T   is the temperature (in kelvin; K).

Example:

From the figure C.1, $\dfrac{-E}{R}$ =   -2,132.4

-E   =   -2,132.4 × 8.314
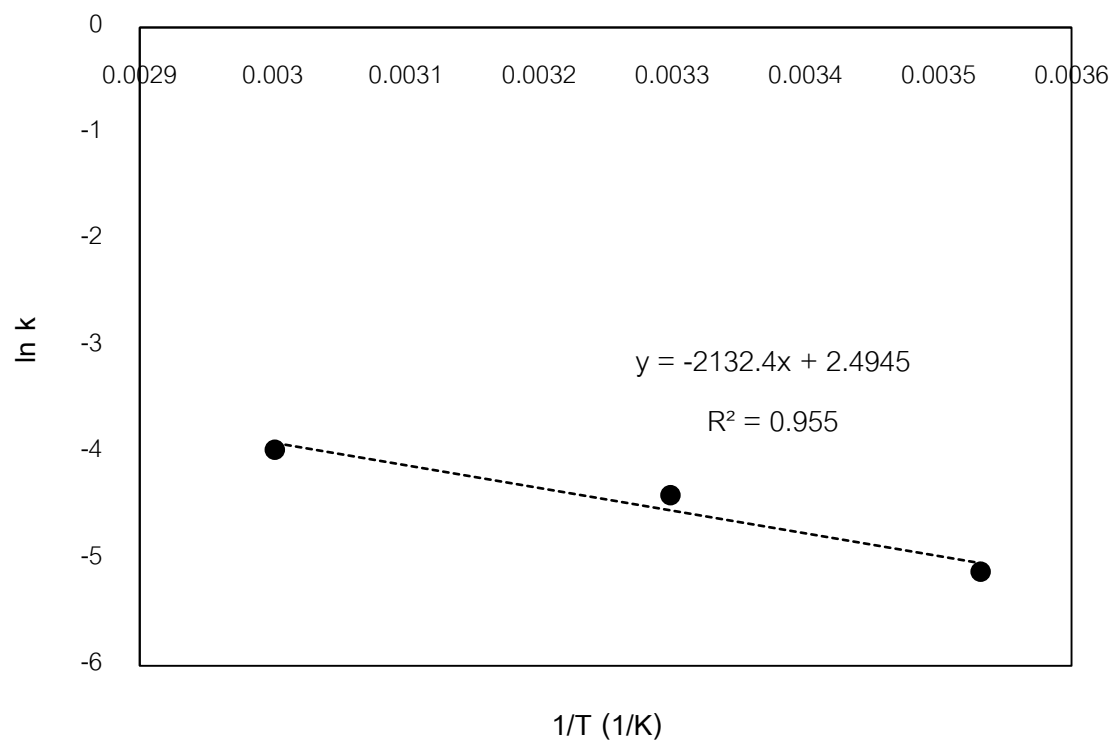
E   =   17,728.7736 J·mol-1.

Figure C.1 The relationship between the reaction rate coefficient and temperature.

APPENDIX D

KINETIC OF REACTION.

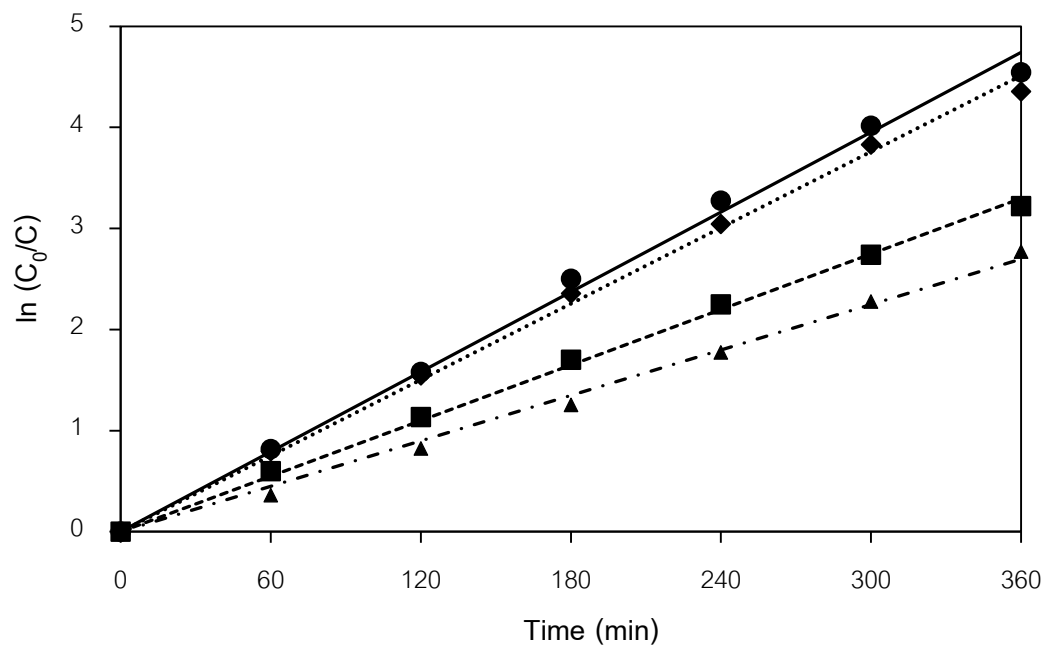**Figure D.1** The kinetic plot of diuron degradation via EAOP on the influence of mixing

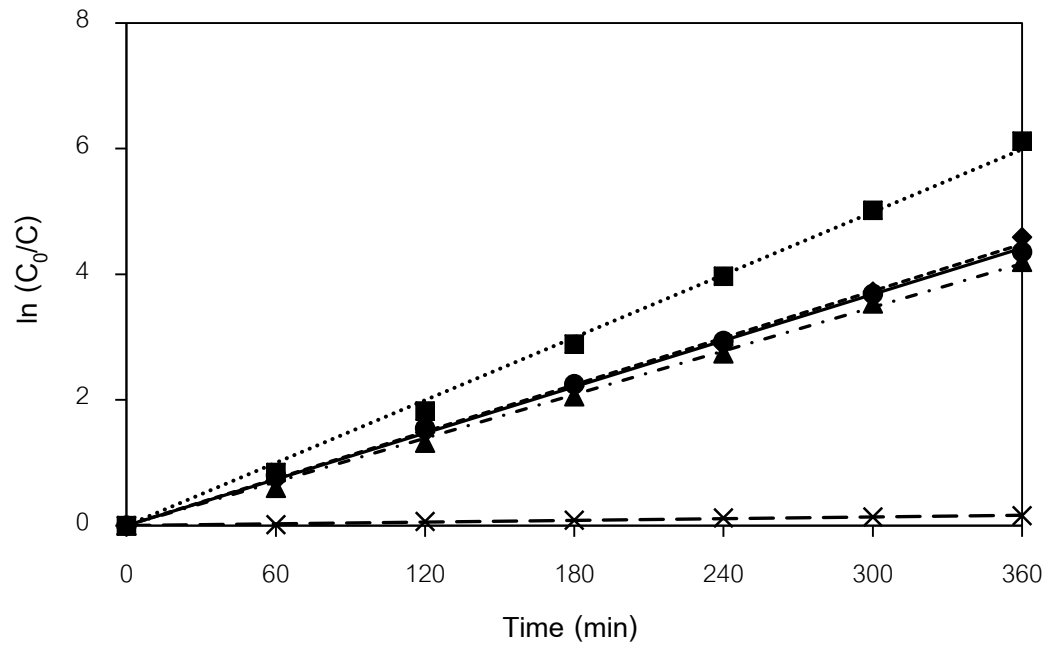speed: (▲) 800 rpm, (■) 1,000 rpm, (◆) 1,200 rpm, and (●) 1,500 rpm.

Figure D.2 The kinetic plot of diuron degradation via EAOP on the influence of electrolyte

type: (▲) NaHCO$_3$, (■) NaCl, (◆) NaNO$_3$, (●) Na$_2$SO$_4$, and (x) no electrolyte.
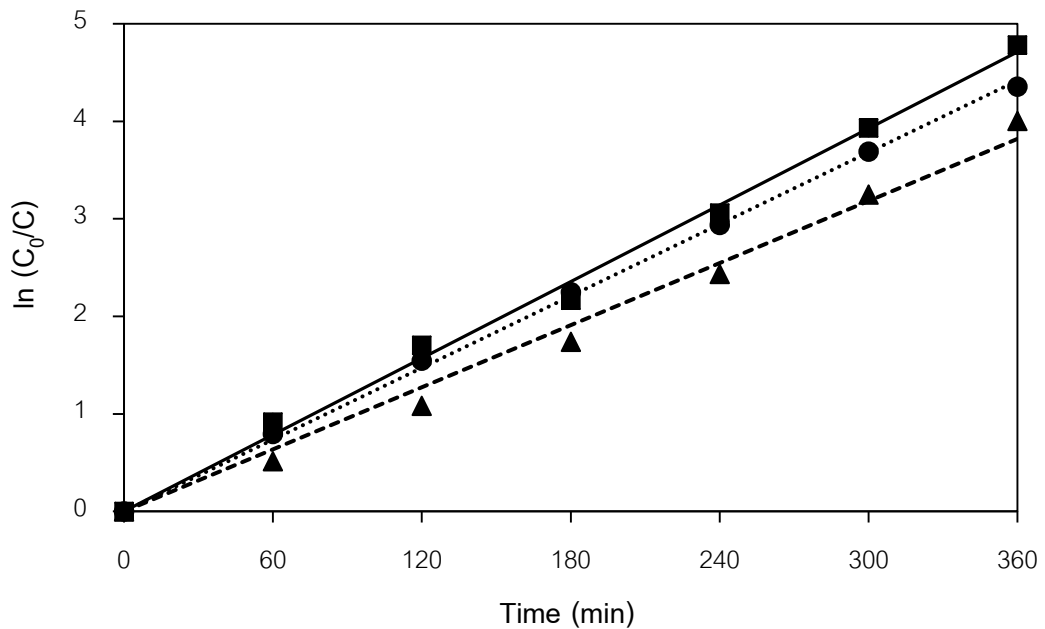

Figure D.3 The kinetic plot of diuron degradation via EAOP on the influence of applied

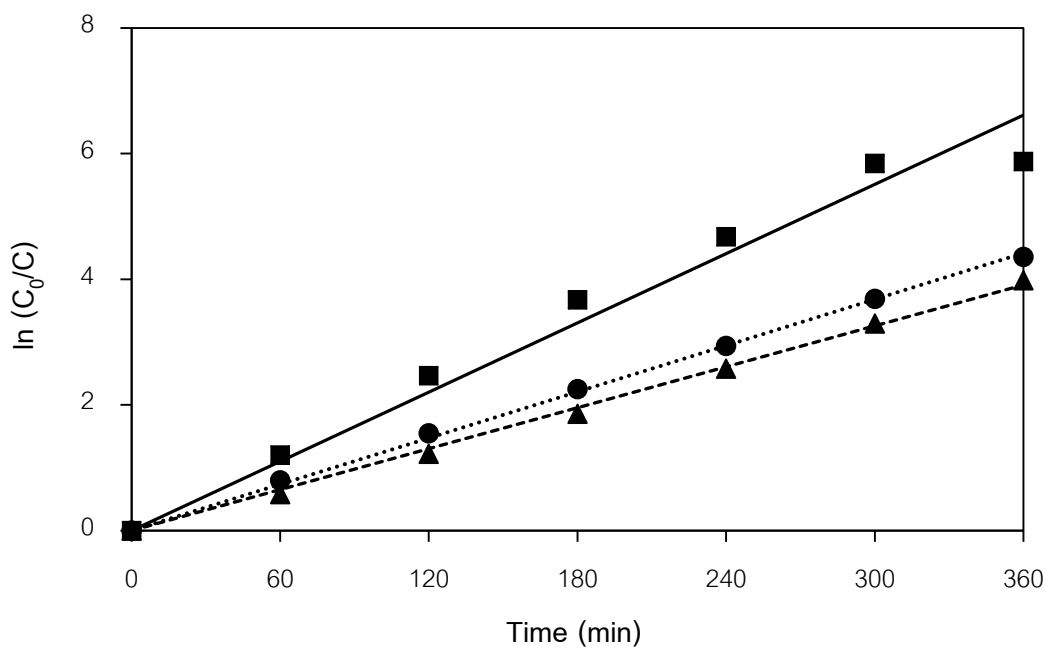electric current: (▲) 30 mA, (●) 50 mA, and (■) 100 mA.

Figure D.4 The kinetic plot of diuron degradation via EAOP on the influence of initial pH: (▲) pH 3, (●) pH 7, and (■) pH 11.
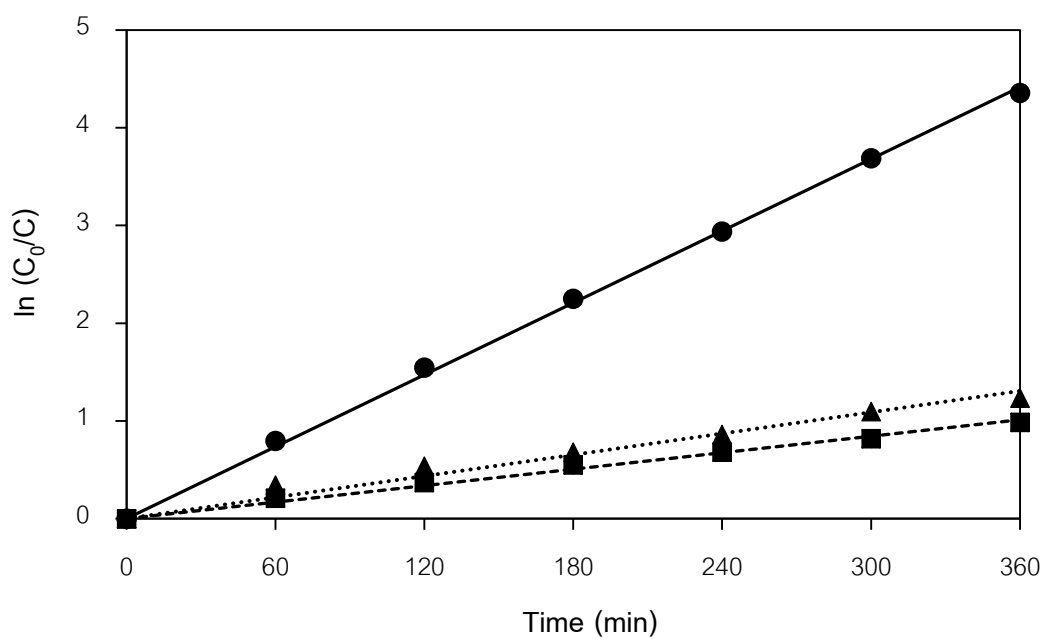

Figure D.5 The kinetic plot of diuron degradation via EAOP on the influence of electrode type: (●) graphite, (■) stainless steel, and, (▲) gold plated stainless steel.
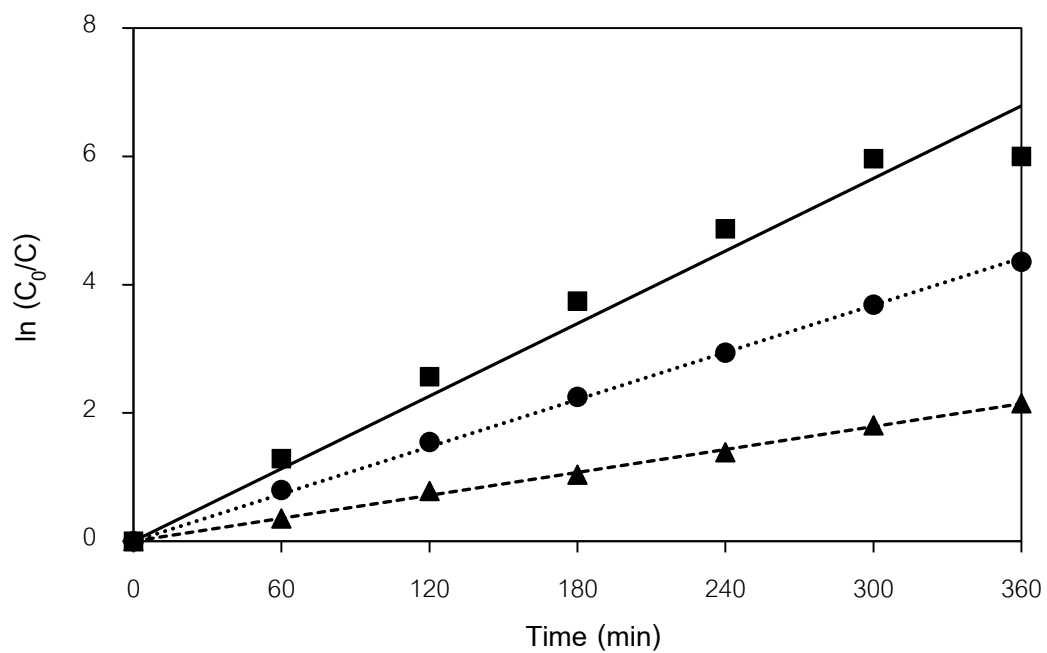
Figure D.6 The kinetic plot of diuron degradation via EAOP on the influence of temperature: (▲) 10 °C, (●) 30 °C, and, (■) 60 °C.

APPENDIX E

CALCULATION OF RATIO OF DIURON AND HYDROXYL RADICAL

Assumptions: - Distance of reaction is 1 µm.

             - Hydroxyl radicals do not recombine to hydrogen peroxide.

             - Hydroxyl radicals generate continuous as linear.

$$\text{Amount mole of } {}^{\bullet}\text{OH} \quad = \quad 2 \times \left(0.05 \, \frac{mg}{L}\right) \times \left(0.55 \, L\right) \times \left(\frac{1 \, mol}{34 \, g}\right)$$

$$= \quad 0.0161 \, mmol$$

$$= \quad \left(\frac{0.0161 \, mmol}{6 \, hr.}\right) \times \left(\frac{1 \, hr.}{3{,}600 \, s}\right)$$

$$= \quad 7.47 \times 10^{-7} \, mol/s$$

$$\text{Volume of reaction} \quad = \quad 2 \times 4.5 \times 4.9 \times 10^{-4}$$

$$= \quad 4.41 \times 10^{-3} \, cm^{3} \, (\, 4.41 \times 10^{-6} \, L)$$

$$\text{Amount mole of diuron} = \quad \left(10 \, \frac{mg}{L}\right) \times \left(4.41 \times 10^{-6} \, L\right) \times \left(\frac{1 \, mol}{233 \, g}\right)$$

$$= \quad 1.89 \times 10^{-7} \, mol$$

$$\text{The ratio of diuron and hydroxyl radical} \quad = \quad \frac{\text{mole of diuron}}{\text{mole of HO}^{\bullet}}$$

$$= \quad \frac{1.89 \times 10^{-7}}{7.47 \times 10^{-7}}$$

$$\approx \quad \frac{1}{4}$$

APPENDIX F

LIST OF PUBLICATION.

1. Panchika Prapakornrattana and Varong Pavarajarn. "Diuron degradation via electrochemical advanced oxidation". Pure and Applied Chemistry International Conference 2016 (PACCON2016), Bangkok, Thailand, February 9-11, 2016.

VITA

Ms.Panchika Prapakornrattana was born on 20 September, 1991, in Bangkok, Thailand. She recieved the Bachelor's degree of engineering with a major in Chemical Engineering from faculty of Engineering, Kasetsart University, Bangkok in March 2014. She continuously entered the Master degree at Center of Excellence in Particle Technology (CEPT), Department of Chemical Engineering, Faculty of Engineering, Chulalongkorn University, Thailand since August 2014.

จุฬาลงกรณ์มหาวิทยาลัย
CHULALONGKORN UNIVERSITY